AN IMPROVED MULTI-VARIATE EMPIRICAL MODE DECOMPOSITION METHOD TOWARDS SYSTEM IDENTIFICATION OF STRUCTURES

by

Mohamed Barbosh

A thesis

submitted to the faculty of graduate studies

in partial fulfilment of the requirement for the

degree of Master of Science

in

Civil Engineering

Lakehead University

Thunder Bay, Ontario

December 2017

© **Mohamed Barbosh**, 2017

Dedicated to my parents and my wife

Table of Contents

List of Tables . . . . . **v**

List of Figures . . . . . **viii**

Abstract . . . . . **ix**

Acknowledgements . . . . . **x**

Chapter 1 Introduction **1**

1.1 Structural Health Monitoring 1

1.2 Literature Review of System Identification 2

1.2.1 Time-domain Methods 3

1.2.2 Frequency-domain Methods 5

1.2.3 Time-frequency domain Methods 6

1.3 Gap Areas 9

1.4 Thesis Objectives 10

Chapter 2 Proposed Algorithm **12**

2.1 Background 12

2.1.1 Empirical Mode Decomposition 12

2.1.2 Multi-variate EMD 14

2.1.3 Independent Component Analysis 18

2.2 Formulation 23

Chapter 3 Numerical Studies **26**

3.1 3-DOF Model 26

3.2 4-DOF Model 30

3.2.1 Low-energy modes 30

3.2.2 Closely-spaced frequencies 35

3.3 10-DOF Model 38

Chapter 4 Full-scale Studies 43

4.1 Experimental Study 43

4.2 Real-life Structural Validation 48

4.2.1 High-rise Tower 48

4.2.2 Long-span bridge 53

Chapter 5 Conclusions and Future Work 61

5.1 Key Conclusions 61

5.2 Major Research Contributions 62

5.3 Future Work 62

5.4 Acronyms 64

Bibliography 65

List of Tables

Table 3.1 Theoretical and identified modal parameters of 3-DOF model . 30

Table 3.2 Theoretical and identified modal parameters of 4-DOF models . 37

Table 3.3 Theoretical and identified modal parameters of 10-DOF model 42

Table 4.1 Accuracy of the identification results in experimental model . . 47

Table 4.2 Daily variation of the identified natural frequencies of the CT tower 53

Table 4.3 Overview of vehicles passing over bridge during each test 57

Table 4.4 Comparison of the identification results with the FE model of long-span bridge 59

List of Figures

Figure 1.1 Steps of the SHM 3

Figure 2.1 Sifting process [38] 14

Figure 2.2 Performance of the MEMD method 17

Figure 2.3 Performance of the MEMD under low energy signals 17

Figure 2.4 Performance of the MEMD under closely spaced signals 18

Figure 2.5 Sine signals and their mixtures 21

Figure 2.6 Estimated sine signals obtained from the ICA 22

Figure 2.7 Flowchart of the proposed method 25

Figure 3.1 3-DOF model 27

Figure 3.2 Fourier spectra of the floor vibration measurements 28

Figure 3.3 IMFs of the first, second and third floor measurements obtained from the MEMD 28

Figure 3.4 (a - b) IMFs with mode-mixing and (c - d) separated IMFs using the ICA 29

Figure 3.5 Damping ratio of the resulting modal responses 29

Figure 3.6 4-DOF systems: model A and B 30

Figure 3.7 Fourier spectra of the floor vibration measurements of model A 31

Figure 3.8 IMFs of the first, second and third floor measurements obtained from the MEMD 32

Figure 3.9 (a - b) IMFs with mode-mixing and (c - d) separated IMFs using the ICA 33

Figure 3.10 (a - b - c) IMFs with mode-mixing and (d - e - f) separated IMFs using the ICA 33

Figure 3.11 Damping ratio of the resulting modal responses 34

Figure 3.12 Fourier spectra of the floor vibration measurements of model B 35

Figure 3.13 IMFs of first, second and third floor from the MEMD 36

Figure 3.14 (a - b - c) IMFs with mode-mixing and (d - e - f) separated IMFs using the ICA 36

Figure 3.15 10-DOF model 38

Figure 3.16 Fourier spectra of the floor vibration measurements of the model 39

Figure 3.17 IMFs of the first, second, third, fourth, sixth and eighth floor measurements obtained from the MEMD 40

Figure 3.18 (a - b - c) IMFs with mode-mixing and (e - f - g) separated IMFs using the ICA 41

Figure 3.19 (a - b - c - d - e - f) IMFs with mode-mixing and (g - h - i - j - k - l) separated IMFs using the ICA 42

Figure 4.1 (a) Experimental model and (b) FE model 44

Figure 4.2 (a) Sample data and (b) Fourier spectrum of 3-th floor response 45

Figure 4.3 IMFs of first, third and fifth sensor as obtained from the MEMD method 46

Figure 4.4 (a - b - c) IMFs with mode-mixing and (d - e - f) separated IMFs using the proposed method 46

Figure 4.5 Modeshapes of the model 47

Figure 4.6 Schematic of sensor locations in the Canton Tower (Ni et al. 2009) 49

Figure 4.7 Fourier spectra of the vibration measurements at 3rd, 9th and 16th floor 50

Figure 4.8 IMFs of the third, fifth, eighth and sixteenth sensor as obtained from the MEMD method 51

Figure 4.9 (a - c) IMFs with mode-mixing and (b - d) the separated IMFs using the proposed method 52

Figure 4.10 Variation of the first two natural frequencies of CT tower over 24 hours 52

Figure 4.11 Long-span bridge in Thunder Bay 53

Figure 4.12 (a) Typical sensor placed on the sidewalk, (b) vehicles passing over the bridge during a test and (c) location of sensors on the bridge 54

Figure 4.13 FE model of the bridge 55

Figure 4.14 Fourier spectra of vibration measurements at various locations 58

Figure 4.15 The IMFs of the second, fourth and sixth sensor from the MEMD 59

Figure 4.16 The IMFs with mode-mixed modal responses and the separated IMFs using the proposed method 60

Abstract

Structural health monitoring (SHM) plays a key role towards condition assessment of large-scale civil structures using modern sensing technology. Once the rich vibration data is collected, important system information is extracted from the data and subsequently such information is used for necessary decision making including adopting maintenance, retrofitting or control strategies. System identification is one of the key steps in SHM where unknown system information of the structures is estimated based on the response measurements. However, depending on excitation characteristics or system behavior, vibration measurements become complicated where traditional methods are unable to accurately analyze the data.

In this thesis, Multivariate Empirical Mode Decomposition (MEMD) method is explored to undertake ambient system identification of structures using the multi-sensor vibration data. Due to inherent sifting operation of EMD, the traditional MEMD results into mode-mixing that causes significant inaccuracy in structural modal identification. In this research, Independent Component Analysis (ICA) method is integrated with the MEMD to alleviate mode mixing in the resulting modal responses. The proposed hybrid MEMD method is verified using a suite of numerical, experimental and full-scale studies (e.g., a high-rise tower in China and a long-span bridge in Canada) considering several practical applications including low energy modes, closely spaced frequencies and measurement noise in real-life buildings and bridges. The results show significantly improved performance of the proposed method compared to the standard EMD method and therefore, the proposed method can be considered as a robust ambient modal identification method for flexible structures.

Acknowledgements

First and foremost, I would like to express my sincere thanks and gratitude to my thesis supervisor, Dr. Ayan Sadhu, for his inspirational guidance and support. Dr. Sadhu has been a wonderful mentor and has provided me with the right attitude and impetus needed to complete this work on time.

My sincere thanks to Dr. Jian Deng and Dr. Carlos Zerpa for serving on my thesis committee. I would also like to thank Dr. Sam Salem for his timely kind assistance as our graduate co-ordinator to organize my thesis seminar and defence.

I would like to thank Tripoli University and the Libyan Education Ministry for their financial support throughout my studies at Lakehead University. I am really grateful to the City of Thunder Bay for providing access to the Main Street bridge and the authority of Guangzhou Tower for sharing its vibration data online. I would like to thank my research team (Mr. Malek Laziri, Mr. Nawaf Almasri, Mr. Chanakya Bodupalli and Mr. Peter Friesen) for their continuous support and assistance during my stay at Lakehead University.

Special thanks are reserved for my father, Mr. Emhemed Barbosh. My father's valuable advice on my early academic study and guidance in shaping up my academic career is gratefully acknowledged. I would also like to thank my mother, my wife, my kids (Maryam and Mosab) and my entire family for their emotional support and encouragement. Without their unwavering support and sacrifice, this work would not have been possible.

Chapter 1

Introduction

1.1 Structural Health Monitoring

Large-scale civil infrastructure such as long-span bridges, tunnels, tall buildings, towers and stadiums have seen a vast growth worldwide in last several decades. Some of these existing aging structures are subjected to damage in the course of their service life due to exposure of a variety of loads such as earthquakes, winds, traffic loads and may lose their structural integrity. This may cause a real danger to the human being (i.e., infrastructure owners, users and operators) due to any undesirable movement or catastrophic failure of existing structures. Structural health monitoring (SHM) is one of the major and accurate tools for early damage detection and finding timely retrofitting of these structures.

The SHM is a diagnostic and prognosis tool developed for continuous monitoring of physical state of structure. It uses a class of methods to analyze the existing state of any structure including the traditional visual inspection method to evaluate the exterior condition of structure, and the vibration-based monitoring system to measure the responses of structure (i.e., displacements, accelerations responses) using the sensor devices. Vibration measurements primarily help to detect early invisible damages, this is why, vibration-based monitoring has become more popular in recent years.

The fundamental idea of vibration-based SHM is that damage can change the

structural parameters such as stiffnesses and frequencies which are clearly appeared in the model responses of the structure. Condition assessment of structure is the prime stage of the SHM that is used to evaluate its current condition, predict early damages and conduct proper maintenance before the failure occurs. Enhancing the safety of structures, avoiding abnormal behavior, and selecting the suitable maintenance strategies can be achieved by adopting appropriate SHM strategies. The SHM was initially developed in offshore field in the 70's of the twentieth century to monitor civil structures in the 80's [1]. The SHM is consisted of four major steps: (a) data collection, (b) system identification, (c) condition assessment and (d) decision making. As shown in Fig. 1.1, once the rich vibration data is collected using sensors, system identification [2] is undertaken that enables to obtain the model parameters (i.e., frequencies, damping and mode shapes) from vibration data and is used to evaluate current condition of the structure. In last few decades, there has been significant research in the area of system identification for civil and mechanical structures addressing a wide range of challenges depending on the structure of interests.

1.2 Literature Review of System Identification

System Identification (SI)[3] is the process of modeling an unknown system based on a set of input and output. The SI is also known as an inverse problem since the main objective is to extract system information from the vibration measurements collected from the structure. The SI is an important tool to evaluate the current performance or safety functions of the structure and recognize the extent of damage due to natural hazards such as earthquake, strong wind or in-service loads. It helps to extract the model parameters using vibration data by estimating the model responses of structures. However, it is very difficult and expensive to measure the excitation

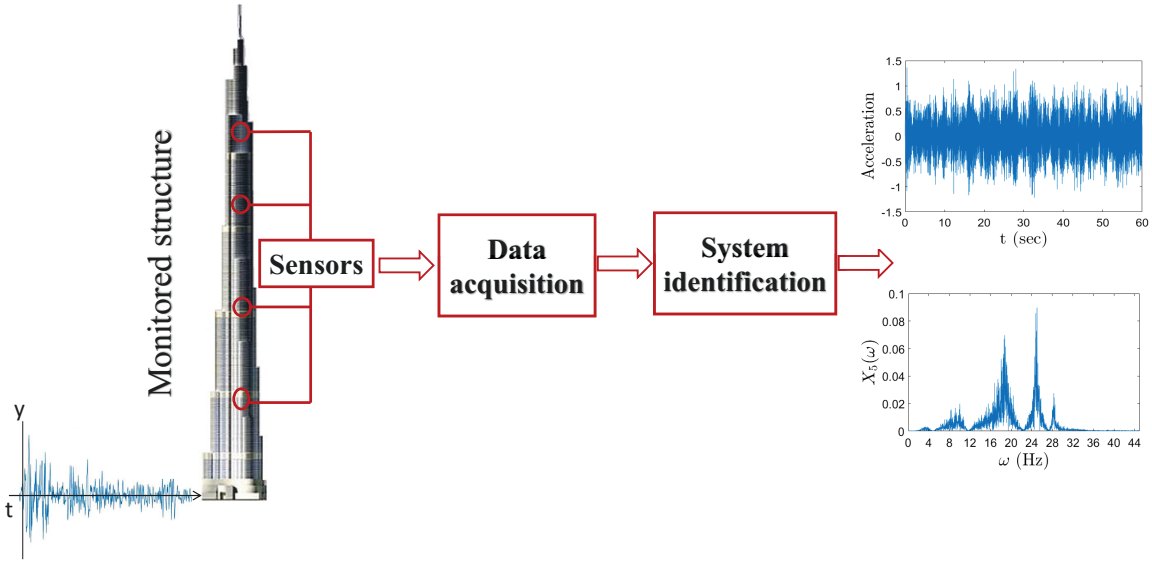

Figure 1.1: Steps of the SHM

(i.e., input) in large-scale infrastructures while it is easier to measure output just by using cheaper sensors. This is why, output-only modal identification has been very popular for civil structures. There are different output-only modal identification techniques [4, 3] used in both structural and mechanical system since early 20's. These techniques work either in the time, frequency or time-frequency domain which are reviewed next.

1.2.1 Time-domain Methods

Among all time-domain methods [5, 6, 8, 7, 19], complex exponential (CE) algorithm based on Prony's method [9] is possibly the first single-input single-output parametric identification technique. The main idea of Prony's method is to obtain the model parameters from a uniformly sampled signal by creating a sequence of damped complex exponentials, or sinusoids using impulse response functions (IRFs). The CE algorithm was then integrated with least-squares (LSCE) [7] to make it suitable for

single-input multiple-output systems.

Expanding the concept of Prony's method, Ibrahim time domain (ITD) method was developed as a modal identification method for single-input single-output systems. The ITD method estimated the modal parameters using free acceleration responses rather using impulse response functions (IRFs). However, the ITD method was computationally expensive. The ITD method was combined with random decrement method to perform modal identification of structural systems [10, 11]. A new method named as poly-reference complex exponential was developed as an extension of the least squares complex exponential (LSCE) algorithm which was used first time as modal identification for multiple-input multiple-output systems [12, 3].

The eigen system realization algorithm (ERA) [8, 4] was developed based on the general state-space description for linear dynamic systems by using impulse response functions. The eigen-value decomposition of the Hankel matrix was used to extract the modal parameters. However, in this method, free or impulse responses of structures were needed which may not be available in some structural systems due to several factors including safety, size, and availability of ambient vibrations. Natural Excitation Technique (NExT) [13] was developed to address this drawback. The NExT can be processed as free responses since it meets the requirement of the homogeneous differential equation of motion [3]. Furthermore, the NExT in conjunction with eigensystem realization algorithm (ERA) was conveniently utilized for structural modal identification lately [13, 14, 15, 4].

Another time-domain method, Stochastic Subspace Identification (SSI), was developed in the early to mid of 1990's [16, 17] that provided a powerful tool of output-only system identification. The stochastic state space system is used as the framework of the stochastic subspace identification method. The SSI technique is suitable in case

of having large number of outputs data [18]. However, SSI method is computationally expensive and time-consuming process as it involves stability diagram and model order pre-selection.

1.2.2 Frequency-domain Methods

The frequency domain methods perform the vibration analysis with respect to frequency, rather than time. Frequency domain techniques are mainly based on frequency response functions [12, 20, 21]. There were two methods developed [12, 3]: rational fraction polynomial based method and Ewins-Glesson method. A power spectra density based on peak picking is another classical frequency domain method was developed by [20, 4]. However, this method was found to be inaccurate to estimate the damping ratios and mode shapes. The frequency domain decomposition (FDD) was a new frequency domain method that was developed to resolve the difficulties encountered in pick picking with retaining the advantages of the classical pick picking method [21, 3]. This method had some useful features over the other frequency domain methods such as processing speed and simplicity.

The classical FDD was extended [22] to identify the symmetrical structures with closely-spaced modes. This technique was based on singular value decomposition of spectra density matrix at power spectra density peaks. However, some issues correlated with FFTs still existed in this method. Thereafter, a new method was proposed to determine the damping ratios using the extended FDD technique [23]. FDD was a simple and computationally faster method, however it was not suitable for high damped systems with closely spaced modes. This is a common case in flexible structures with supplemental damping devices such as active and tuned mass dampers (TMDs). Lately, there has been a significant growth in signal processing that led to

the development of powerful system identification using time-frequency techniques.

1.2.3 Time-frequency domain Methods

Time-frequency domain methods [24] present a picture of frequency and time domain information simultaneously. In last two decades, time-frequency domain methods have gained significant attention especially in civil and mechanical systems. The methods including wavelet transform (WT) [25, 28, 30, 26, 27, 29], blind source separation (BSS) [31, 32, 34, 3, 33] and empirical mode decomposition (EMD) [38, 35, 36, 37] are used as modal identification methods for large-scale civil infrastructure.

Wavelet Transform (WT) method [26, 29] provides a useful transformation to represent signals by using a suitable basis functions that satisfy certain properties of linear vector spaces in $\Re^3$. This method has gained significant popularity in structural applications [25, 29]. The use of sinusoidal basis in Fourier transform restricts the non-stationary response of system, which makes its usage limited to ambient system identification. Since the Fourier basis functions are localized in frequency only, a new method called short-time Fourier transform (STFT) was proposed to provide the time-varying information of signals. However, the achievable time and frequency resolutions are considerably restrained due to fixed nature of the windows used in STFT.

Similar to Hiesenberg's uncertainty principle, it is impossible to achieve good time and frequency resolutions at same time. This prompted the development of an alternative method that produced a preferred time-frequency representation of the signals in a multi-resolution framework, known as wavelet transform (WT). This method results in accurate representation of vibration measurement because of its compactness, quick decaying characteristics, and higher order moments. With such properties, the

useful information content of the signal is preserved while the casual contributions from noise are discarded. This gives sufficient time-frequency representation of the signals and makes them more compact, smooth and noise free [40]. The wavelet transform of a signal $x(t)$ is a linear transform which can be defined as:

$$w_k^j(x) = \frac{1}{\sqrt{j}} \int_{-\infty}^{\infty} x(t)\ \psi_k^{j*}(t)\ dt \tag{1.1}$$

Where the function ψ is known as the mother wavelet and $*$ stands for complex conjugation. k and j indicate translation and scale parameters, respectively. Thus, wavelet transform decomposes a signal $x(t)$ through basis functions that are essentially scaled and translated versions of the mother wavelet (ψ). There are two categories of wavelet transforms, redundant and non-redundant wavelet transforms. Discrete wavelet transform (DWT) belongs to the former category, whereas continuous wavelet transforms (CWT) and stationary wavelet transforms (SWT) belong to the later [42, 43, 41].

The separation of original source signals from their observed mixed signal without knowing system information and the source signals, is known as blind source separation (BSS). BSS is a powerful tool that is widely used in many different fields of science and engineering [43, 34]. BSS can be utilized to recover a linearly mixed sources from just their observed mixtures. All of that can be achieved by using the output signal only [44, 43]. The BSS was lately used as inverse problems for ambient structural modal identification [34, 31, 45]. In general, there are two popular tools to solve the BSS problems: Independent Component Analysis (ICA) and Second-Order Blind Identification (SOBI). While the ICA method utilizes high-order statistics to separate the inherent signals, the SOBI method uses the second-order statistics like covariance matrices of vibration measurements for the decomposition [33].

Empirical Mode Decomposition (EMD) is one of the time-frequency decomposition tools that can deal with both nonlinear and nonstationary signals [47] without requiring any basis functions. Owing to this property, it has gained significant popularity in the area of structural condition assessment and damage detection. The EMD method was originally developed by Huang et al. [38] that creates a set of intrinsic mode functions (IMF) representing time and frequency domain information of the signal. The EMD is also known as an adaptive time-frequency decomposition method that decomposes a multi-component signal into a number of mono-component signals. The IMFs are extracted by sifting operation that is undertaken by multiple averaging and interpolation operations of the raw signal. However, sifting operations cause considerable mode mixing in the IMFs [35]. Recently a wavelet-bounded EMD [54] is proposed to find an optimization-based solution to the problem of mode-mixing.

Unlike the WT and BSS, the EMD method is self-adaptive in nature [38]. Furthermore, the EMD method can deal with a single real-valued signal to obtain a subset of modal responses [56]. However, the standard EMD method is not suitable for multivariate vibration data [58, 48]. While dealing with vibration measurements from multiple sensors of a large structure, the EMD method faces mode-mixing problem [47, 37]. In order to alleviate this limitation, the EMD method is extended to a method called multivariate EMD (MEMD) which is appropriate for multichannel data measurements [48]. The MEMD treats any signal as n-variate multidimensional time series and decomposes its inherent components along suitable directions in a multidimensional space. In order to estimate all possible envelopes [59], the multiple signals are projected to the chosen direction vectors, and then the average of all envelopes is taken as a local mean of multiple signals.

An integrated MEMD method [37] is recently developed where ensemble EMD

(EEMD) is used to inject artificial noise repeatedly to the measured signal eliminating the effect of mode-mixing in the modal responses of the MEMD. However, the EEMD method has several limitations especially for large-scale structures associated with higher computational time and intensive signal processing [57, 37]. Moreover, the MEMD method is never validated under a wide range of practical situations including closely-spaced frequencies, measurements noise and vibration measurements of full-scale structures. This thesis integrates MEMD with the ICA [55] to solve the mode-mixing problem while dealing with the multichannel vibration measurements of large-scale structures. The ICA method is perfectly suitable to deal with multichannel measurement with lesser computational time and results in improved performances of the MEMD under closely-spaced modes and low energy frequencies due to the higher-order analysis. Apart from numerical and experimental studies, the performance of the proposed method is validated using two real-life structures showing the efficacy of the MEMD first time in the full-scale civil infrastructure.

1.3 Gap Areas

- Large scale structures have several low energy modes in vibration response which are difficult to identify using traditional model identification methods. Such situations primarily occur due to inadequate energy in high frequency modes under ambient vibration or improper placement of sensors throughout the structures.

- Structural systems have closely-spaced frequencies in the modal responses which is another major challenge in system identification using traditional methods. Presence of control devices (e.g. tuned mass dampers) or symmetrical configuration of structures result in such closely-spaced modes. Structural retrofitting or vibration control requires accurate modal identification of these structures.

- Traditional methods are time-intensive and incapable of separating mode-mixed modal responses of vibration data.
- The existing methods are not robust to measurement noise and result in significant inaccuracy when applied to large-scale structures.
- In spite of its popularity, the EMD is suitable only for single channel measurement. There is a need to develop a robust EMD method that can utilize multiple sensor measurements together and avoid separate data processing of each channel of measurements.

1.4 Thesis Objectives

With above mentioned gap areas of the existing literature of modal identification methods, the main objectives of this thesis are summarized as follows:

- Develop a new time-frequency algorithm for modal identification of structures addressing the issues of low energy modes and closely-spaced frequencies.
- Develop a robust EMD method that can perform accurate modal identification using multi-channel vibration measurements without introducing any mode mixing.
- Demonstrate and validate the proposed method to several numerical, laboratory and full-scale structures under a wide range of practical situations.
- The proposed method should be also robust with respect to measurement noise present in the vibration sensors.

The thesis is outlined as follows. First, a background of EMD, MEMD and ICA is presented in **Chapter 2** followed by the formulation of the proposed algorithm.

In **Chapter 3**, numerical simulation are conducted using a wide range of dynamical models subjected to various excitation. Experimental and full-scale studies using a high-rise tower and large-span bridge are conducted in **Chapter 4**. Finally the key conclusions of the proposed research are discussed in **Chapter 5** followed by the the major research contributions and future work.

Chapter 2

Proposed Algorithm

In this chapter, a multi-variate EMD (MEMD) algorithm is explored as a possible tool for modal identification. The proposed method is derived from the equation of motion of a dynamical system using the classical theories of structural dynamics. Unlike EMD, the MEMD uses multi-channel measurement data to perform system identification. In order to alleviate the mode-mixing issue of EMD (as explained in the previous chapter), Independent Component Analysis (ICA) is utilized to extract mono-component modal responses from the mode-mixed results obtained from the MEMD.

2.1 Background

In this section, a brief background of the EMD, MEMD and ICA method is presented first before going into the details of the proposed algorithm.

2.1.1 Empirical Mode Decomposition

Empirical mode decomposition (EMD) [38] is a time-frequency domain signal decomposition technique that has gained significant popularity in the area of output-only modal identification of structures [56]. The EMD method decomposes an original signal into a set of oscillatory waveforms named as intrinsic mode functions (IMFs) that are intended to be single frequency components. An IMF is a function that satisfies following two conditions: (1) the number of extrema and the number of zero-crossings

have to be either equal or differ at most by one in the whole data set, and (2) at any point, the mean value of the envelope denoted by the local maxima and the local minima is zero. The procedure of extracting an IMF is called $sifting$ (see Fig. 2.1). Suppose $x(t)$ is the signal to be decomposed, the main steps of EMD are as follows:

- Connect all the local maxima and the local minima by using a cubic spline in order to shape the upper and lower envelops.
- Determine the mean of upper and lower envelops which is designated as $c_1(t)$. Then, find the difference between the signal $x(t)$ and the mean $c_1(t)$, $i_1(t) = x(t) - c_1(t)$ which could be first IMF.
- Check whether $i_1(t)$ satisfies the two conditions of IMF that are mentioned above. If $i_1(t)$ satisfies the both conditions to be an IMF, then $i_1(t)$ is the first IMF of the original signal $x(t)$.
- If $i_1(t)$ does not satisfy the requirements of IMF, the sifting process will be repeated by treating the $i_1(t)$ as original signal until it meets the two conditions of IMF.
- The original signal subtracted from the IMF, and the sifting process is repeated to decompose the data into m IMFs [38].

Finally, the signal $x(t)$ can be expressed as :

$$x(t) = \sum_{j=1}^{m} i_j(t) + r_m(t) \tag{2.1}$$

Where $i_j(t)$ $(j = 1, 2, 3, ..., m)$ represents the IMFs of the original signal $x(t)$ and $r_m(t)$ is a single value function that represents the residue of $x(t)$. Ideally, every IMF must has only one frequency component. However, sometimes one IMF contains several frequency components which are known as *mode-mixing*.

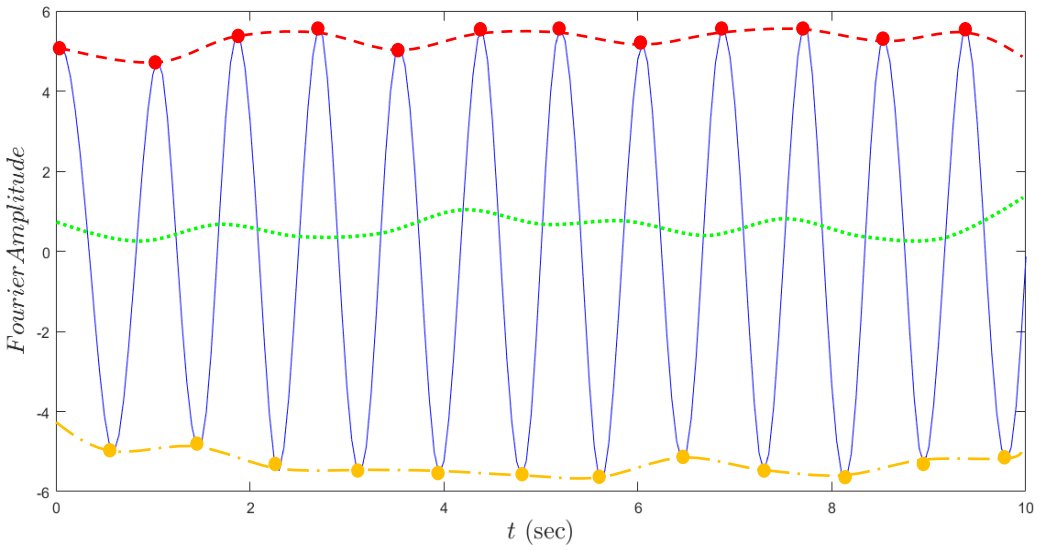

Figure 2.1: Sifting process [38]

2.1.2 Multi-variate EMD

As mentioned in previous chapter, the traditional EMD method is suitable just for analyzing single data measurement. EMD faces significant issues while dealing with multiple data measurements [38]. Furthermore, the joint information between multiple sensors can not be utilized due to the individually treated signals at each sensor locations. In order to address this limitation, the standard EMD was recently extended to its multivariate form which is perfect for multichannel signal [46]. In the MEMD method, the multidimensional envelops are generated by taking signal projections along different directions, and then the local mean of signals can be obtained by taking the average of these envelops. In case of analyzing n-dimensional signal, quasi-Monte Carlo lower deviation sequence is used in order to create a group of uniformly distributed points on a unit (n-1)-sphere [48, 47]. In case of dealing with n-dimensional signal $x(t) = [x_1(t), x_2(t), ..., x_n(t)]$, and $D^k = [d_1^k, d_2^k, ..., d_n^k]$ is the direction vectors along the k-th direction, the MEMD is performed using these

steps below [48]:

(a) choose an appropriate group of direction vectors, D.

(b) determine the k-th projection , denoted by $p^k(t)$ of the input signal $x(t)$ over the k-th direction vector, X^k, for all k (k=1,2,.....,L, where L is the number of direction vectors D).

(c) find the moment t_i^k of maximum $p^k(t)$ for all k for all k.

(d) interpolate $[t_i^k, y(t_i^k)]$ to obtain multi-dimensional envelopes, $e^k(t)$ over all k.

(e) calculate the mean of envelope, $M(t)$ for a set of L direction vectors:

$$M(t) = \frac{1}{L}\sum_{k=1}^{L} e^k(t) \tag{2.2}$$

(f) extract the residual $R(t)$ using $R(t) = x(t) - M(t)$. If $R(t)$ satisfies the stopping criteria of multivariate IMF, repeat the above steps to $[x(t) - R(t)]$ until the next order IMF is diminished. Otherwise repeat it to $R(t)$.

In order to illustrate how the MEMD works, a simple example involving a mixture of sine signals (see Eq. 2.3) is considered where $\omega = \{1.1, 2.3, 3.7\}$ Hz, respectively.

$$A = \begin{bmatrix} 7 & -3 & 5 \\ -4 & 7 & -5 \\ 3 & -5 & 7 \end{bmatrix} \begin{bmatrix} \sin(\omega_1 t) \\ \sin(\omega_2 t) \\ \sin(\omega_3 t) \end{bmatrix} \tag{2.3}$$

The measurement noise with SNR = 10 is also added in the mixtures. Then the MEMD is applied on the three mixtures, and the extracting IMFs of each mixture $x_i(t)$ for $i = 1, 2, 3$ are shown in Fig. 2.2. First column of Fig. 2.2 contains the IMFs of first mixture $x_1(t)$, second column contains the IMFs of $x_2(t)$ and third column contains the IMFs of $x_3(t)$. In order to check the accuracy of the estimated IMFs, each $x_i(t)$ is reconstructed using the IMFs and compared with the original mixtures.

it can be observed that the estimated signals totally match with the actual signals as shown in the fourth row of Fig. 2.2.

It may be noticed that Eq. 2.3 is equivalent to the modal superposition of the structural systems where the sine signals represent the modal responses and **A** is the corresponding mode shape matrix. In general, there are many low energy modes in the vibration responses of a tall flexible civil structure. Low energy modes occur due to either placed of sensors on *nodes* which have zero displacements, presence of higher modes or mass/stiffness distributions of the structure. It is quite difficult to identify such low energy and closely spaced modes in modal responses.

In order to simulate such low energy modes case, the amplitude of the sine wave that has frequency value 2.3 Hz (see Eq. 2.3) is decreased by multiplying it by factor of 0.1. Then the MEMD is used to separate the sources. Fig. 2.3 shows the typical results of the identified IMFs and it can be observed that IMF-3 of all measurements contains a substantial amount of mode mixing due to its low energy contents in the vibration measurements.

Most of structural systems are often equipped with closely-spaced modes due to the symmetrical geometry or the existence of tuned-mass dampers. In order to simulate such closely-spaced situations, the frequencies of the signals in Eq. 2.3 are changed to 0.8, 1.3 and 2.3 Hz and the MEMD is employed to separate the sources. The identification results under closely spaced signals are shown in Fig. 2.4 and it can be seen that the signals are containing significant amplitude and frequency modulations in the separate signals. Both Figs. 2.3 and 2.4 are the key results and give the basic motivation to develop a robust MEMD method which can perform structural modal identification using the vibration measurements containing low energy modes,

closely spaced modes and measurement noise. It will be shown later how the proposed method can be employed to perform modal identification of large-scale real-life structures under these situations.

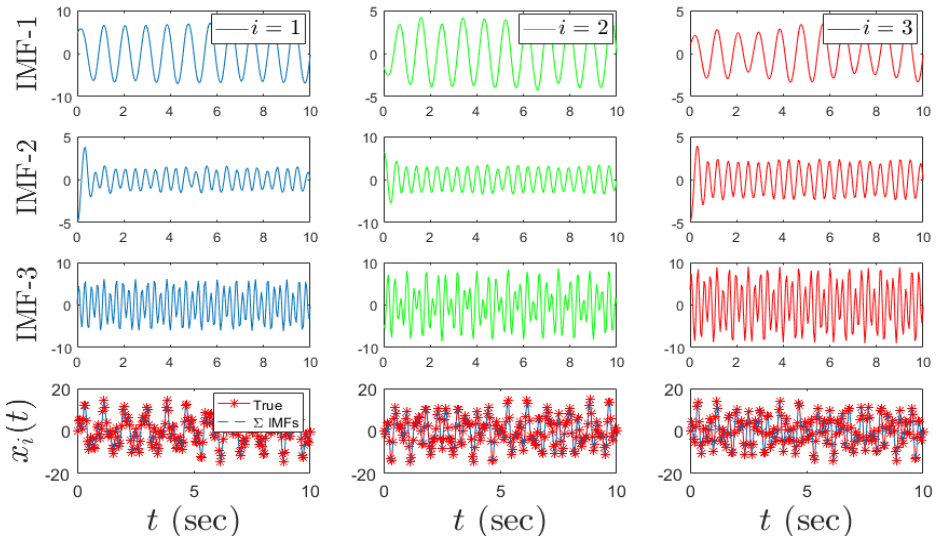

Figure 2.2: Performance of the MEMD method

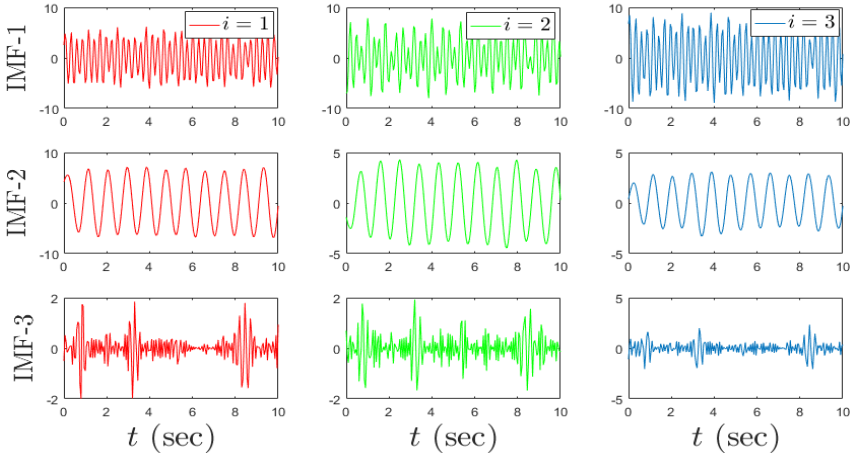

Figure 2.3: Performance of the MEMD under low energy signals

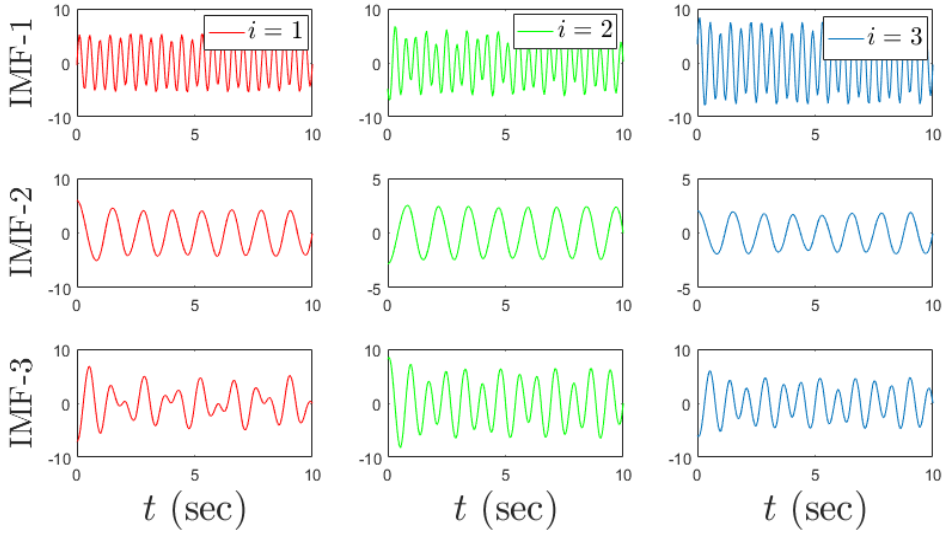

Figure 2.4: Performance of the MEMD under closely spaced signals

2.1.3 Independent Component Analysis

Independent Component Analysis has gained a wide popularity for performing blind source separation [49] of acoustic or bio-medical signals. In the ICA, the observed signals are assumed to be linear combination of statistically independent sources. The ICA decomposes a multiple measurements into independent non-Gaussian signals [50]. In case of analyzing multi-component signal that is consisted of several mono-component signals from different sources, it is possible to separate those participating sources from the mixed signals. The ICA of any random signal $\mathbf{x}(t)$ is extracted by estimating a $n \times m$ full order separating matrix $\mathbf{W}$ with $n \leq m$ and then the output signal vector can be expressed by:

$$\mathbf{y}(t) = \mathbf{W}\mathbf{x}(t) \tag{2.4}$$

Where $\mathbf{y}(t)$ is totally independent in statistical sense. Therefore, the independence can be computed by the information theoretic cost function such as maximization of cumulants [49]. The ICA method is based on three main principles: (a) the sources are

independent to each other, (b) each source signal has non-Gaussian distribution, and (c) un-correlatedness. Following is a brief discussion of each of these three primary principles of the ICA.

(a) Statistical Independence

This criteria assumes that the sources should be statistically independent. Without this assumption, it is not possible to separate the hidden sources. For instance, lets say there are two source signals $s_1(t)$ and $s_2(t)$ then the first implication is that $s_1(t)$ and $s_2(t)$ are temporally uncorrelated. As a rule, this is not enough requirement to provide a suitable solution. Moreover, it is possible to check that sets $\{s_1(t) + s_2(t)\}$ and $\{s_1(t) - s_2(t)\}$ are independent whereas clearly not being the standard solution. The most significant description of statistical independence of two random components $s_1(t)$ and $s_2(t)$ is expressed by:

$$p(s_1(t), s_2(t)) = p(s_1(t)) \cdot p(s_2(t)) \tag{2.5}$$

where $p(s_1(t))$ reveals the probability density function of the component $s_1(t)$. However, signals are independent when their joint density function can be factorized.

(b) Non-Gaussianity

In the ICA, the source signals have to be non-Gaussian. In order to achieve this, the Central Limit Theorem is used by utilizing the contrast functions such as kurtosis and negentropy. The Central Limit Theorem shows that a sum of independent random variables tends toward Gaussian distribution. However, to extract a source, the main step is to increase the non-Gaussianity of a linear combination of signals which ensures that the individual source is distant away from a Gaussian distribution compared to the mixture of sources.

(c) Whitening

As a main step of the ICA, it is important to whiten the data where the signal can be de-correlated by whitening. It is basically a transformation that gives the covariance matrix of the signals an identity matrix. Whitening performs a significant role in achieving the statistical independence condition. As uncorrelated Gaussian signals are also independent, satisfying non-Gaussianity and whitening automatically satisfy statistical independence.

With above brief background of the ICA, lets see how the ICA can be performed to extract mono-component signal from a mixed signal and how it can be effective in the framework of the MEMD. In Eq. 2.6, the source signals $\mathbf{s}$ (i.e., independent components) are multiplied with the mixing matrix $\mathbf{A}$ to form the mixed signal $\mathbf{x}$.

$$\mathbf{x} = \mathbf{A}\mathbf{s} \tag{2.6}$$

In the ICA model, the challenge is to separate both $\mathbf{A}$ and $\mathbf{s}$ using just $\mathbf{x}$ where the higher order statistics including kurtosis, mutual information or non-Gaussianity are utilized, respectively [50]. After finding $\mathbf{A}$, its inverse is computed (i.e., $\mathbf{W} = \mathbf{A}^{-1}$) that can be used to estimate the independent components by, $\mathbf{y} = \mathbf{W}\mathbf{x}$, where $\mathbf{y}$ is the estimated source vector.

The weight vectors can be estimated by using [43]:

$$\mathbf{W}(N+1) - \mathbf{W}(N) = \eta \mathbf{F}(\mathbf{y})\mathbf{W}(N) \tag{2.7}$$

Where, η is the learning rate that controls the speed of convergence and the matrix $\mathbf{F}(y)$ contains the objective function based on the selected measure of independence (i.e., non-Gaussianity, negentropy or mutual information), for example $\mathbf{F}(y) = A_n - f(y)g^T(y)$ with appropriate chosen nonlinearities $f(y) = [f(y_1), ..., f(y_n)]$ and $g(y) =$

$[g(y_1), ..., g(y_n)]$ [51]. With a prior known knowledge of the source distributions $p_i(y_i)$, $\mathbf{W}$ can be estimated by utilizing the principle of maximum likelihood with the following likelihood function,

$$J(\mathbf{y}, \mathbf{W}) = -\frac{1}{2} \log(|\det(\mathbf{W}\mathbf{W}^T)|) - \sum_{i=1}^{n} E\ \{\log(p_i(y_i))\} \tag{2.8}$$

In general, stochastic gradient method of optimization [51] is used to solve above optimization function and estimate the demixing matrix $\mathbf{W}$.

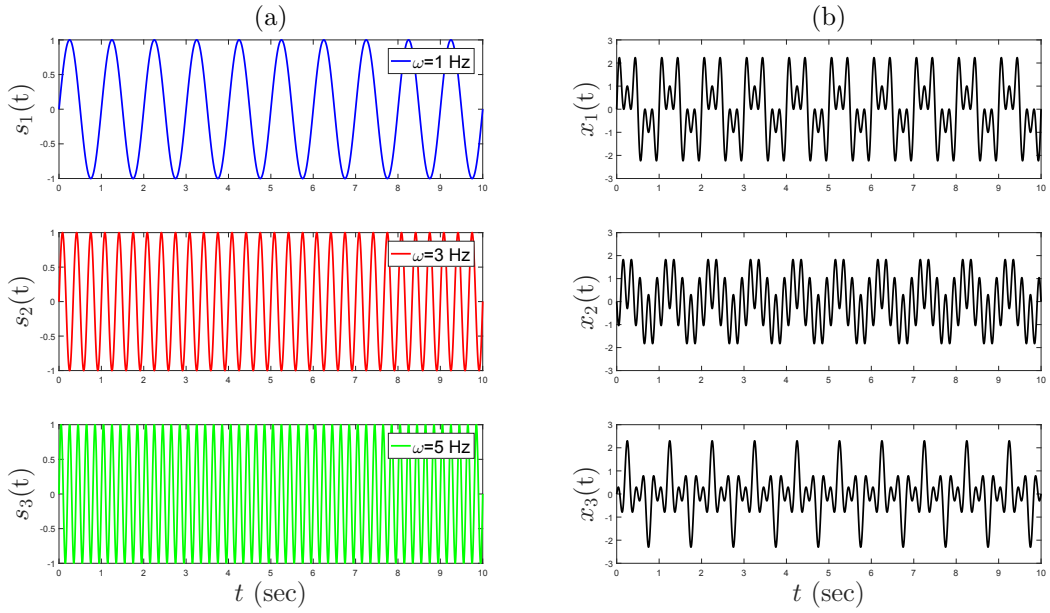

Figure 2.5: Sine signals and their mixtures

The ICA method has excellent capability of separating the signals from their determined or overdetermined mixtures. Moreover, it is relatively fast and computationally less expensive. This is why, the ICA is chosen to separate the signals from their mode-mixed components. In order to demonstrate the signal decomposition capability of the ICA, a mixture of three sine signals is considered next. Fig. 2.5 (a) shows sine signals with frequencies 1, 3 and 5 Hz, respectively and Fig. 2.5 (b) shows the mixtures of the sine signals. These multi-component signals are then decomposed using the ICA. The results of the ICA are shown in Fig. 2.6. It can be observed that the estimated signals in Fig. 2.6 are identical to the original signals as shown in Fig. 2.5(a) which corroborates with the accuracy of the ICA method.

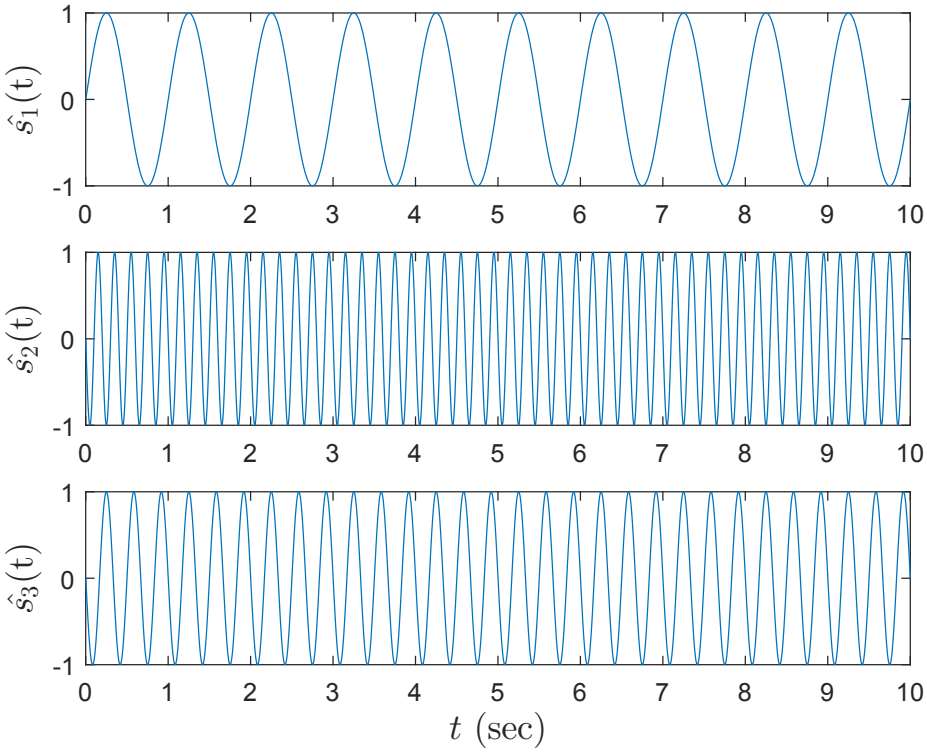

Figure 2.6: Estimated sine signals obtained from the ICA

2.2 Formulation

With the brief background of MEMD and the ICA, let us now formulate the proposed method from the basic equation motion of a dynamical system. Consider a linear, classically damped and lumped-mass n degrees-of-freedom (DOF) structural system, subjected to a wide-band random input force, $\mathbf{F}(t)$:

$$\mathbf{M}\ddot{\mathbf{x}}(t) + \mathbf{C}\dot{\mathbf{x}}(t) + \mathbf{K}\mathbf{x}(t) = \mathbf{F}(t) \tag{2.9}$$

where, $x(t)$ is a vector of displacement response at the DOF. $\mathbf{M}$, $\mathbf{C}$ and $\mathbf{K}$ are mass, damping and stiffness matrix, respectively. The solution to Eq. 2.9 for those of broad-band $\mathbf{F}(t)$ can be written in terms of an expansion of vibration modes:

$$\mathbf{x} = \mathbf{\Psi}\eta \tag{2.10}$$

where, $\mathbf{x}$ and η is the response and modal coordinate matrix, respectively. $\mathbf{\Psi}_{m\times n}$ is the modal transformation matrix. n and m is the number of modal responses and measurements, respectively. The measurement at the i-th DOF ($i = 1, 2, ..., m$) of Eq. 2.10 can be expressed as

$$x_i(t) = \sum_{j=1}^{n} \psi_{ij}\eta_j(t) \tag{2.11}$$

Performing MEMD of $\mathbf{x}(\mathbf{t})$, we can express each signal of $\mathbf{x}(\mathbf{t})$ in terms of its IMFs (i.e., I_{ij}):

$$x_i(t) = \sum_{j=1}^{n} I_{ij}(t) \tag{2.12}$$

where I_{ij} is the j-th IMF of $x_i(t)$. Considering the similarity of Eq. 2.11 and Eq. 2.12, we get [37]:

$$I_{ij}(t) = \psi_{ij}\eta_j(t) \qquad i = 1, 2, ..., m \tag{2.13}$$

Eq. 2.13 relates the IMFs of i^{th} measurement with its modal responses. Therefore, following the same logic for $i = p$ and $i = r$ in Eq. 2.13, the partial mode shape coefficients of p^{th} sensor measurement normalized with respect to the r^{th} measurement is:

$$\frac{I_{pj}}{I_{rj}} = \frac{\psi_{pj}\eta_j}{\psi_{rj}\eta_j} = \frac{\psi_{pj}}{\psi_{rj}} = \bar{\psi}_{pr}; \qquad j = 1, 2, ..., n \tag{2.14}$$

Then, $\bar{\psi}_{pr} = \frac{\psi_{pj}}{\psi_{rj}}$ represents the estimated normalized mode shape coefficient of the j^{th} mode at the p^{th} DOF w.r.t r-th mode. Therefore, we get:

$$I_{pj} = \bar{\psi}_{pr} I_{rj} \tag{2.15}$$

Where, the true value of $\bar{\psi}_{pr}$ can be estimated [37]:

$$\psi_{pr} = \frac{|\rho_{pr}|}{\rho_{pr}} \frac{\sigma_p}{\sigma_r} \tag{2.16}$$

Where, ρ_{pr} is the cross-correlation coefficient.

With this procedure, the normalized mode shape coefficients can be estimated using IMFs of sensor measurements. As discussed in the previous sections, mode-mixing results in due to (a) the repetitive averaging process of EMD , (b) multiple measurements in MEMD, (c) low energy contents and closely-spaced frequencies in the vibration. However, Eq. 2.15 and Eq. 2.16 are valid only when the IMFs are mono-component signals. In order to identify the mono-component sources in the IMFs, the cross-correlation between I_{pj} and I_{rj} is used, and if more than one source is detected, the ICA method is used to find the mono-component IMFs among the mode-mixing IMFs. In this paper, the performance of MEMD is improved by integrating it with the ICA used to eliminate the presence of mode-mixing in the modal responses.

For a mixture of two sources ($j = e, f$) present in I_{ij} as in Eq. 2.13, it can be expressed as,

$$I_{pj} = \psi_{pe}\eta_e + \psi_{pf}\eta_f \tag{2.17}$$

$$I_{rj} = \psi_{re}\eta_e + \psi_{rf}\eta_f$$

Above equation can be written in a matrix form and formulated as the ICA model as shown in Eq. 2.6,

$$\bar{\mathbf{I}} = \bar{\psi}\bar{\eta} \tag{2.18}$$

$$\bar{\mathbf{y}} = \mathbf{W}\bar{\mathbf{I}} = \mathbf{W}\bar{\psi}\bar{\eta} \tag{2.19}$$

Where $\mathbf{W}$ is an unknown matrix that can be estimated using Eq. 2.7. The proposed method is illustrated using the flowchart as shown in Fig. 2.7.

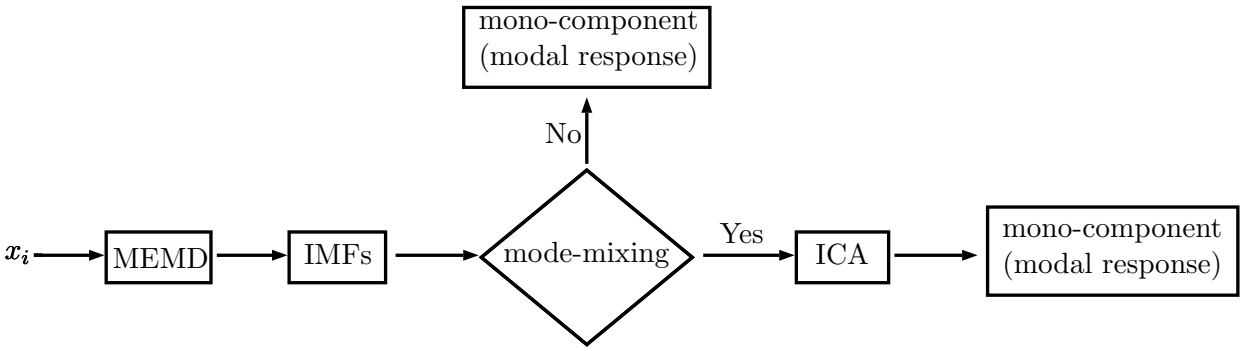

Figure 2.7: Flowchart of the proposed method

Chapter 3

Numerical Studies

In this chapter, the proposed method is validated using three different numerical simulation models with a wide range of dynamical characteristics. The properties of these models are chosen such that the proposed method can be suitably checked with respect to the low energy modes, closely-spaced frequencies and measurement noise.

3.1 3-DOF Model

A 3-storey structure model as shown in Fig. 3.1 is simulated to demonstrate the methodology, and present the key results of the proposed method. The lumped mass and stiffness are assumed to be 144 tonne and 2×10^8 N/m, respectively in each floor, and a modal damping of 5% is considered. The resulting natural frequencies are 2.65, 7.44 and 10.75 Hz, respectively. The model was excited by Imperial Valley earthquake at its base.

Fig. 3.2 shows the Fourier spectra of floor vibration measurements. It can be observed that the 2nd and 3rd modes have significantly low energy compared to the first mode. Fig. 3.3 shows the Fourier spectra of the resulting modal responses obtained from the vibration measurements by using the MEMD method revealing that the modal responses contain both mono-component as well as mode-mixed signals. For example, it can be observed that the first IMFs in all floors (i.e., first row of Fig. 3.3) are all mono-components. However, other IMFs (i.e., in second row of Fig. 3.3) have mode-mixed modal responses. In order to extract the mono-component modal

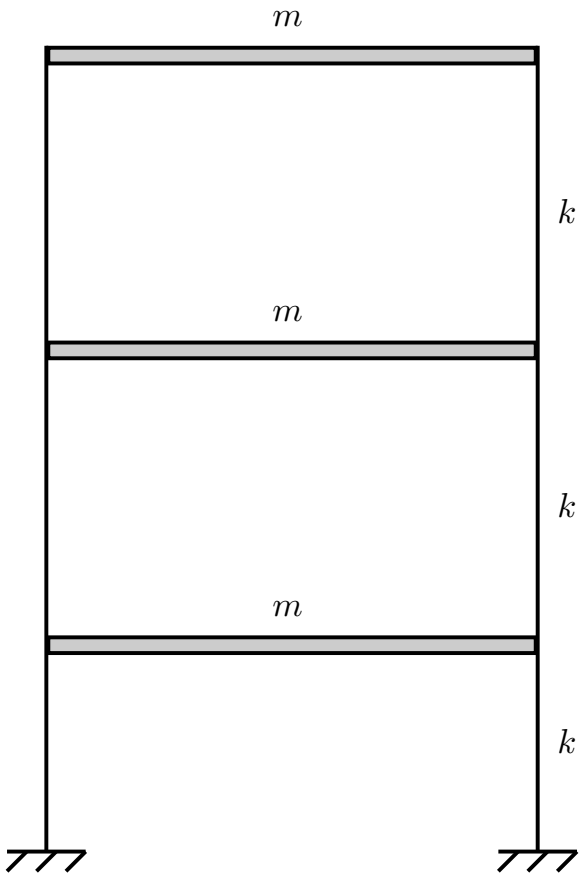

Figure 3.1: 3-DOF model

responses, the ICA is then applied in the mode-mixed IMFs that are highlighted in red box.

The resulting ICA components (i.e., extracted modal responses) of these IMFs are shown in Fig. 3.4. Fig. 3.4 (a) and (b) show the IMFs with mode-mixing resulting from the MEMD that are highlighted in Fig. 3.3 (red box). Fig. 3.4 (c) and (d) show the separated IMFs using the ICA. Once the modal responses are extracted using the proposed method, auto-correlation function of modal responses are used to extract the modal damping ratio. Fig. 3.5 shows the estimation of damping ratio as obtained from the IMFs. Table 3.1 shows the identification results revealing the efficiency of the proposed method under low energy modes.

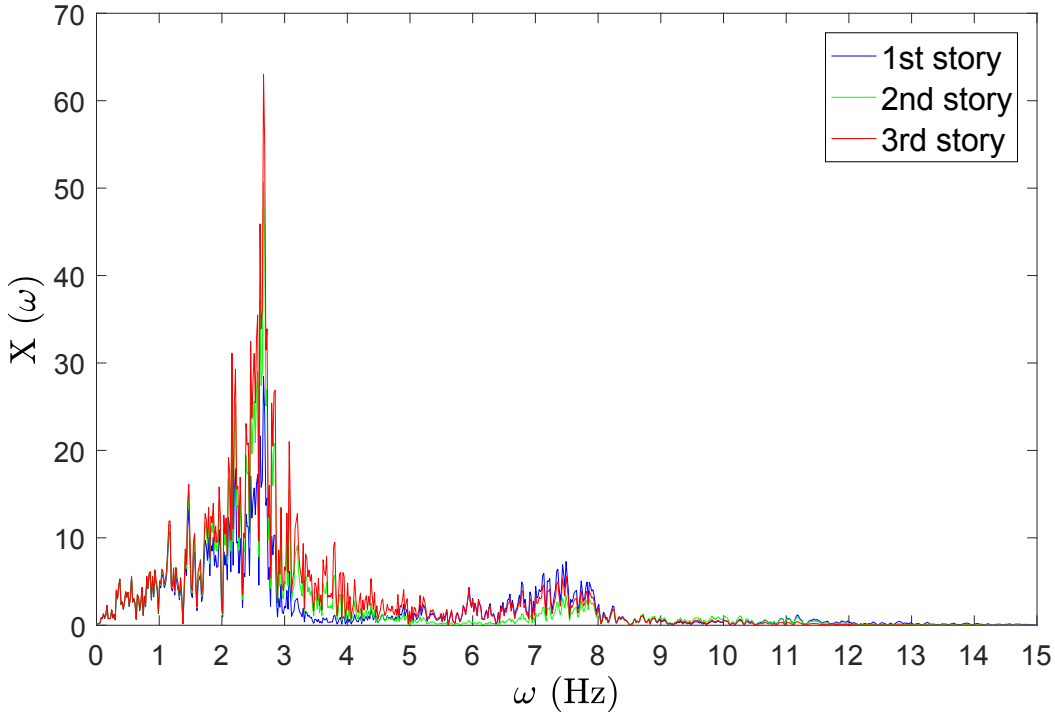

Figure 3.2: Fourier spectra of the floor vibration measurements

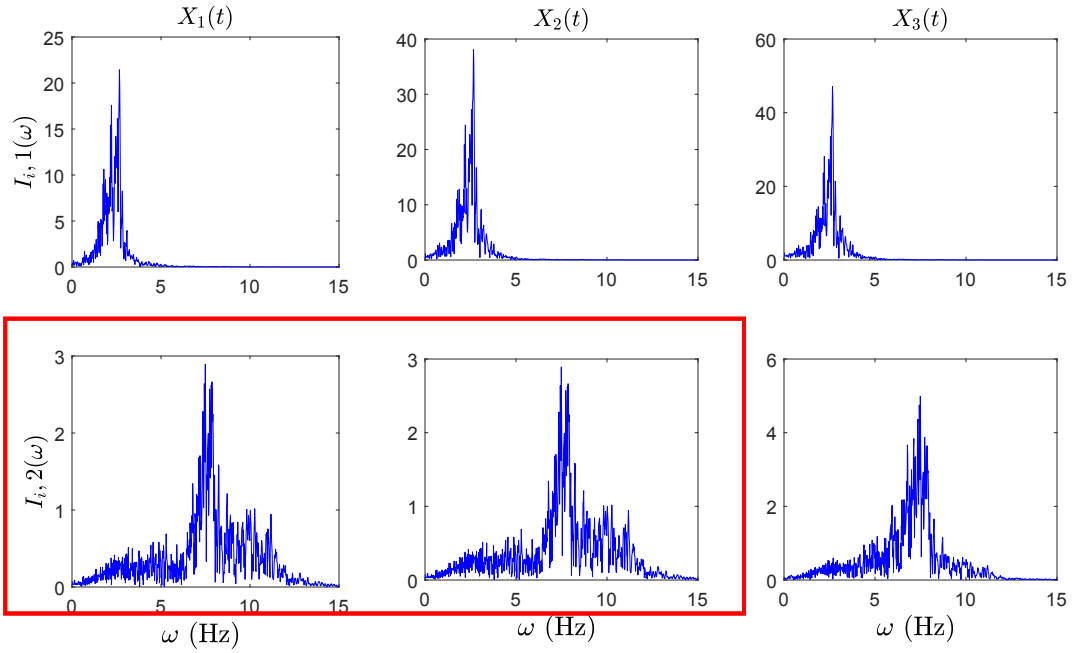

Figure 3.3: IMFs of the first, second and third floor measurements obtained from the MEMD

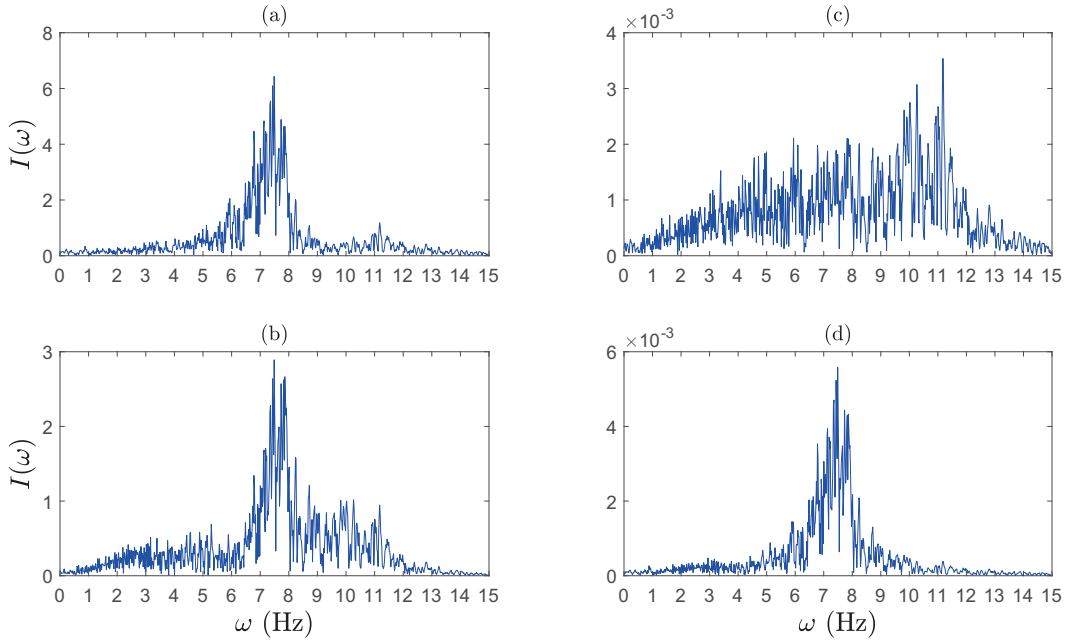

Figure 3.4: (a - b) IMFs with mode-mixing and (c - d) separated IMFs using the ICA

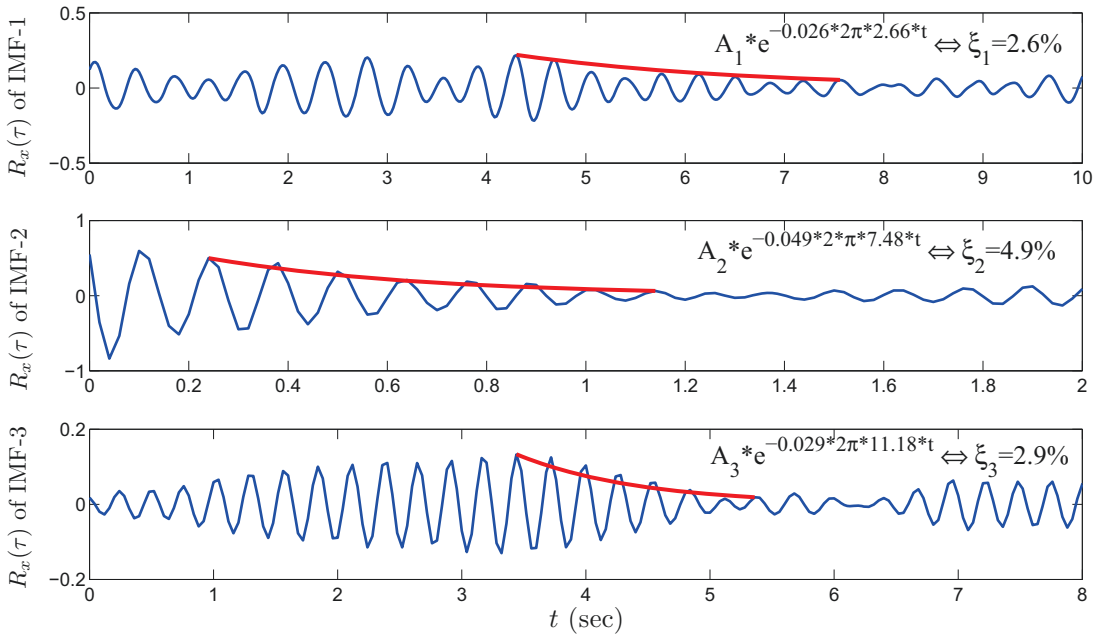

Figure 3.5: Damping ratio of the resulting modal responses

Table 3.1: Theoretical and identified modal parameters of 3-DOF model

Mode #	1	2	3
ω_i (Hz)	2.65	7.44	10.75
$\hat{\omega}_i$ (Hz)	2.66	7.48	11.18
$\hat{\zeta}_i$ (%)	2.6	4.9	2.9

3.2 4-DOF Model

A 4-DOF dynamical system is now considered as shown in Fig. 3.6 [52]. Two different models (i.e., model A and model B) are used to show the effectiveness of the proposed method under low energy modes and closely spaced frequencies, respectively.

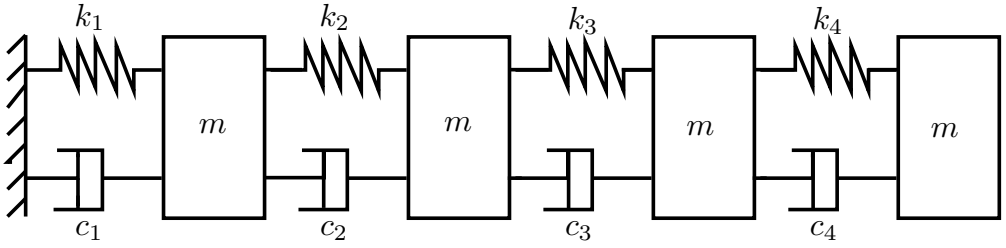

Model A: $m = 1$ Kg, $k_1 = k_3 = 7000$ N/m and $k_2 = k_4 = 8000$ N/m

Model B: $m = 5$ Kg, $k_1 = k_3 = 1000$ N/m and $k_2 = k_4 = 1500$ N/m

Figure 3.6: 4-DOF systems: model A and B

3.2.1 Low-energy modes

In model A, the lumped mass is assumed to be 1 kg in each floor, and a modal damping of 2% is considered. The resulting natural frequencies are 4.74, 13.59, 21.5 and 25.94 Hz, respectively. Fig. 3.7 shows the Fourier spectra of floor vibration measurements. It can be observed that the 3rd and 4th modes have significantly low energy compared to the other modes.

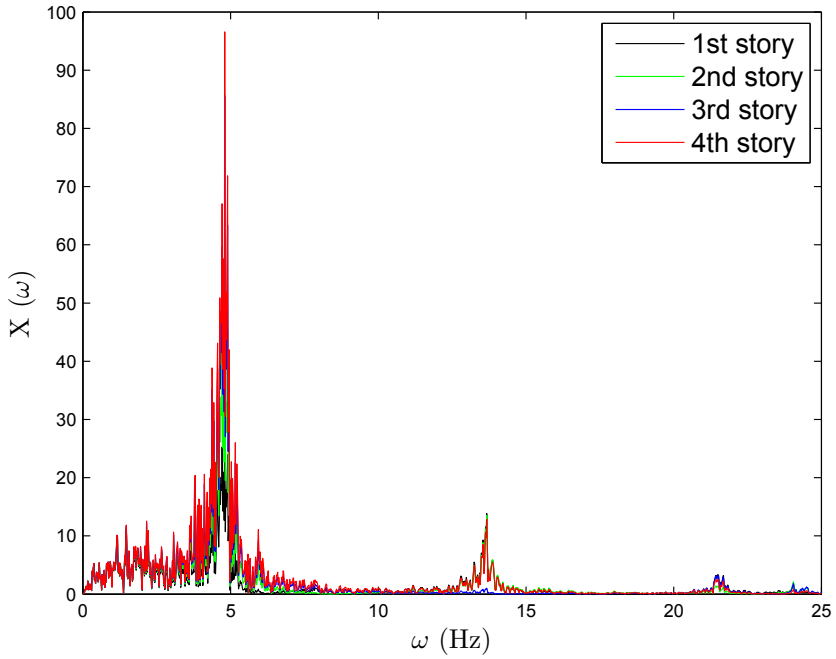

Figure 3.7: Fourier spectra of the floor vibration measurements of model A

Fig. 3.8 shows the Fourier spectra of the resulting modal responses obtained from the vibration measurements by using the MEMD method revealing that the modal responses contain both mono-component as well as mode-mixed signals. For example, it can be observed that the first IMFs in all floors (i.e., first row of Fig. 3.8) are all mono-components. However, other IMFs (i.e., in second and third row of Fig. 3.8) have mode-mixed modal responses. In order to extract the mono-component modal responses, the ICA is then applied in the mode-mixed IMFs that are highlighted in black and red boxes. The resulting ICA components (i.e., extracted modal responses) of these IMFs are shown in Fig. 3.9 and Fig. 3.10, respectively. Fig. 3.9 (a) and (b) show the IMFs with mode-mixing resulting from the MEMD that are highlighted in Fig. 3.8 (black box). Fig. 3.9 (c) and (d) show the separated IMFs using the ICA. Similarly, Fig. 3.10 (a), (b) and (c) show the IMFs with mode-mixing of 1st, 2nd and 3rd floor as obtained from the MEMD that are highlighted in Fig. 3.8 (red box).

Fig. 3.10 (d), (e) and (f) show the separated IMFs using the ICA. As shown in Fig. 3.9 (c-d) and Fig. 3.10 (d-e-f), the proposed method has successfully separated the modal responses of model A even with extremely low energy modes.

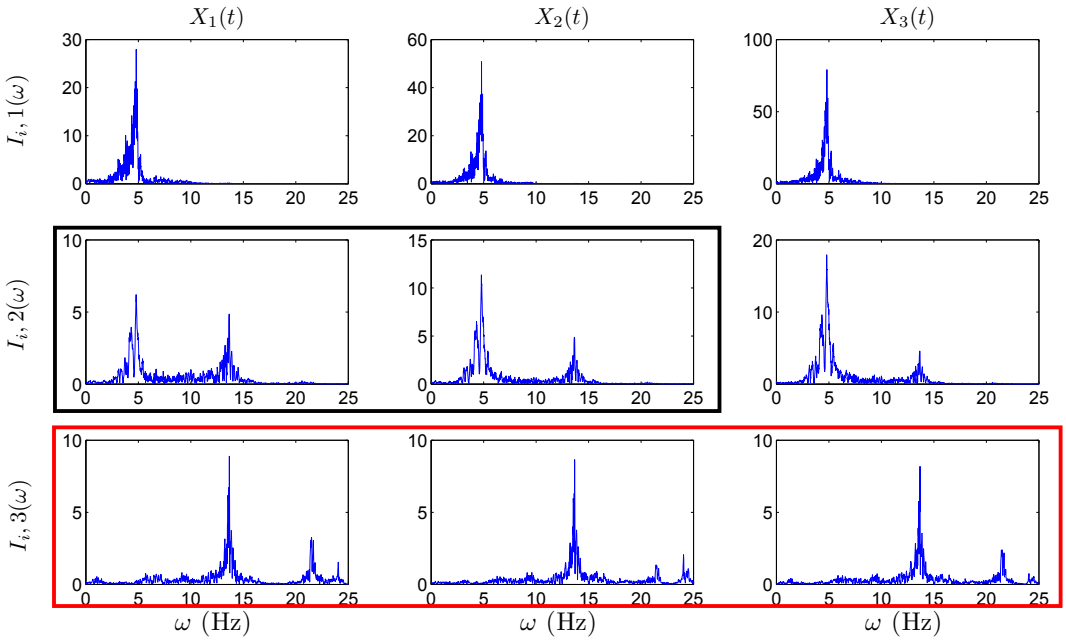

Figure 3.8: IMFs of the first, second and third floor measurements obtained from the MEMD

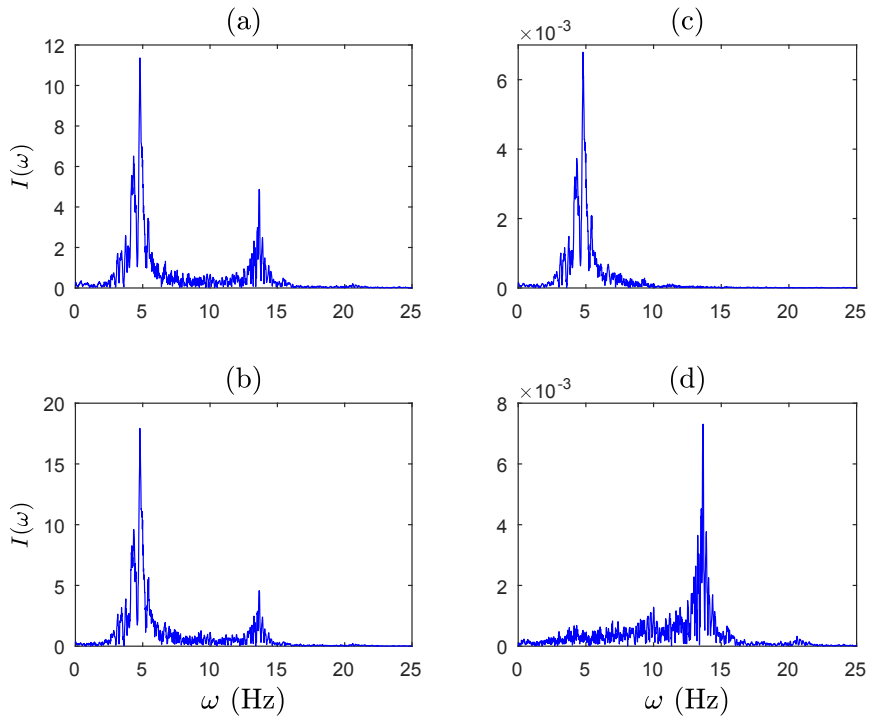

Figure 3.9: (a - b) IMFs with mode-mixing and (c - d) separated IMFs using the ICA

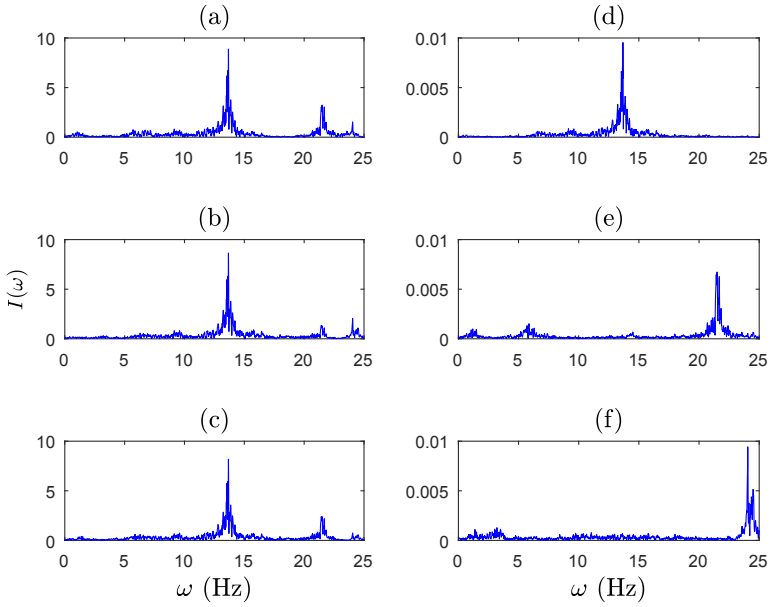

Figure 3.10: (a - b - c) IMFs with mode-mixing and (d - e - f) separated IMFs using the ICA

Once the modal responses are extracted using the proposed method, auto-correlation function of modal responses are used to extract the modal damping ratio. Fig. 3.11 shows the estimation of damping ratio as obtained from the IMFs. Similarly analysis is conducted using the data contaminated with 10 % measurement noise. Table 3.2 shows the summary of the identification results under 0% and 10 % noise revealing the efficiency of the proposed method under measurement noise.

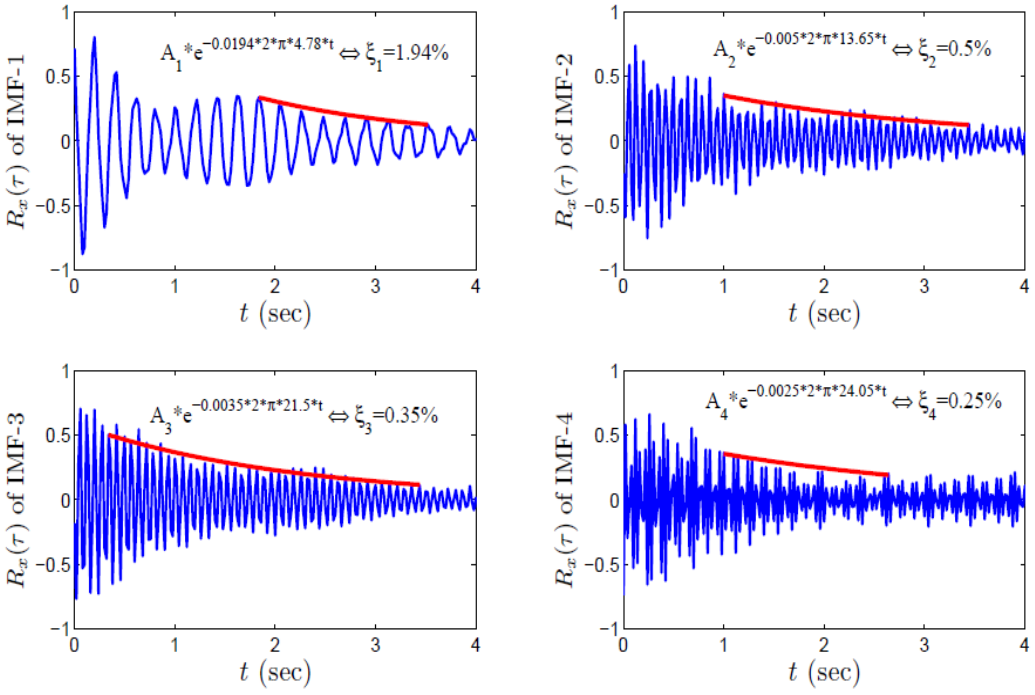

Figure 3.11: Damping ratio of the resulting modal responses

3.2.2 Closely-spaced frequencies

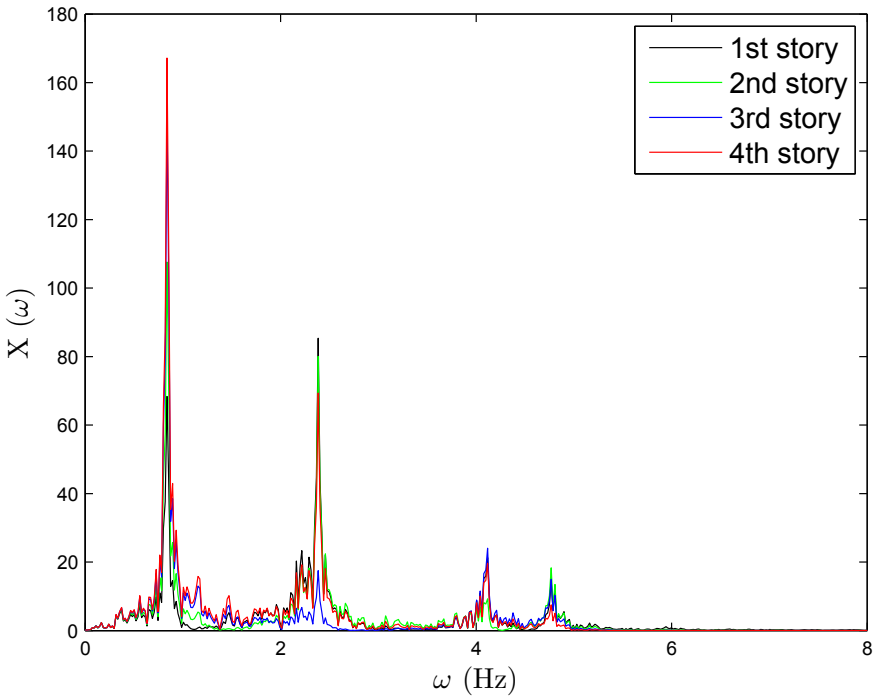

Figure 3.12: Fourier spectra of the floor vibration measurements of model B

In order to simulate the closely-spaced frequencies, model B is created using 5 kg as a lumped mass of the system at each DOF and stiffness as presented in Fig. 3.6. The Fourier spectra of floor vibration measurements is shown in Fig. 3.12. It can be observed that the last two frequencies (i.e., 4.1 and 4.75 Hz) are very closely-spaced. The proposed method is then applied and Fig. 3.13 shows Fourier spectra of the resulting modal responses obtained from the MEMD of vibration measurements. It shows that modal responses contain both mono-component and mode-mixed signals. It can be observed that IMFs in first and second row of Fig. 3.13 are mono-components. However, IMFs in third row of Fig. 3.13 have mode-mixed modal responses. In order to extract the mono-component modal responses, ICA is applied in the mode-mixed IMFs that are highlighted in red box. The resulting ICA components are shown in

Fig. 3.14.

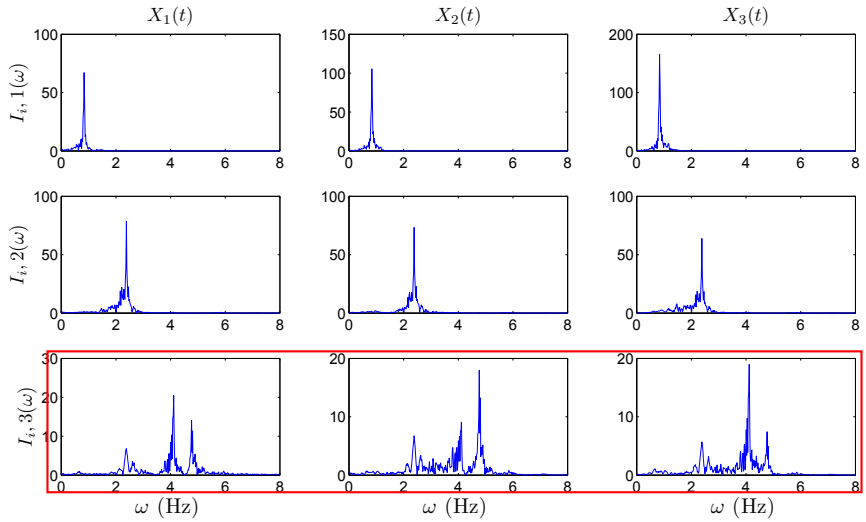

Figure 3.13: IMFs of first, second and third floor from the MEMD

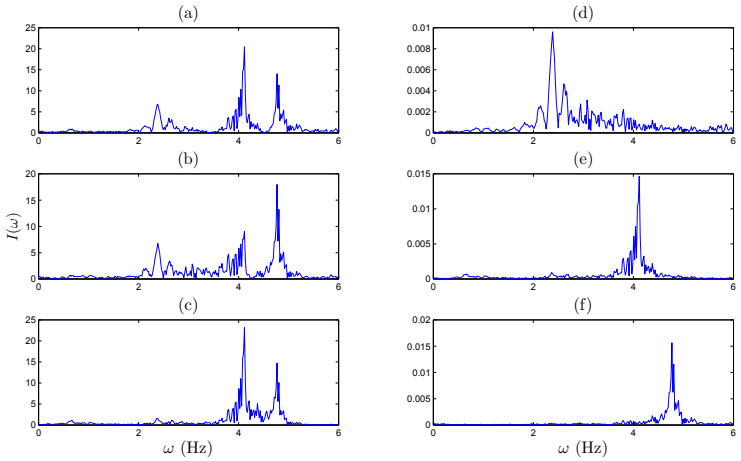

Figure 3.14: (a - b - c) IMFs with mode-mixing and (d - e - f) separated IMFs using the ICA

Fig. 3.14 (a), (b) and (c) show the IMFs with mode-mixing of 1st, 2nd and 3rd modes as obtained from the MEMD that are highlighted in Fig. 3.13 (red box). Fig. 3.14 (d), (e) and (f) show the separated IMFs using the ICA. It can be seen that the closely spaced signals are successfully separated by using the proposed method. The resulting modal parameters are compared with their true values in Table 3.2 with different level of measurement noise.

Table 3.2: Theoretical and identified modal parameters of 4-DOF models

Model A					**Model B**				
Actual	0 % noise		10 % noise		Actual	0 % noise		10 % noise	
(ω_i)	$\hat{\omega}_i$	$\hat{\zeta}_i$ (%)	$\hat{\omega}_i$	$\hat{\zeta}_i$ (%)	(ω_i)	$\hat{\omega}_i$	$\hat{\zeta}_i$ (%)	$\hat{\omega}_i$	$\hat{\zeta}_i$ (%)
4.74	4.78	1.94	4.80	1.93	0.83	0.83	1.52	0.84	1.3
13.59	13.65	0.50	13.67	0.53	2.37	2.38	0.43	2.38	0.6
21.50	21.50	0.35	21.4	0.30	4.07	4.11	0.3	4.12	0.26
25.94	24.05	0.25	24.0	0.16	4.75	4.76	0.23	4.77	0.18

3.3 10-DOF Model

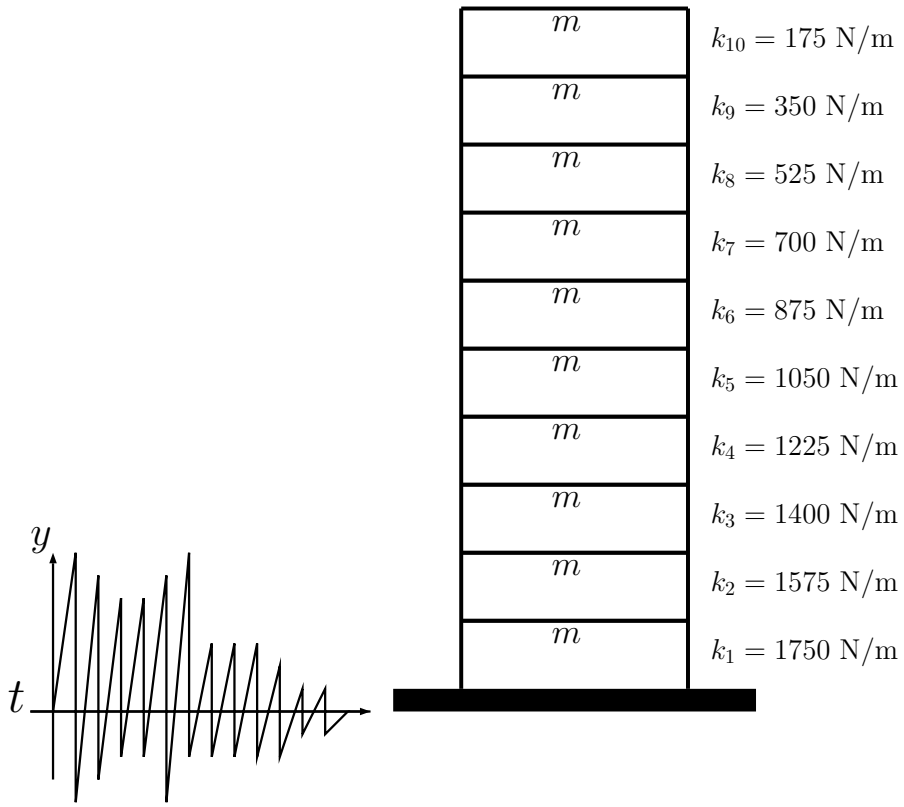

Figure 3.15: 10-DOF model

In order to demonstrate the proposed method with larger DOFs, simulations are now performed on a 10-storey simulation model as shown in Fig. 3.15. For this example building, the lumped mass of each floor is assumed to be 1 kg, and the damping is assumed to be 2% critical in all modes. The natural frequencies are obtained as 0.78, 1.79, 2.83, 3.88, 4.96, 6.07, 7.24, 8.49, 9.87 and 11.51 Hz using eigen-value decomposition of the theoretical mass and stiffness distribution. The 10-DOF building model is excited by Borrego earthquake at its base. Fig. 3.16 shows the Fourier spectra of floor vibration measurements where it can be clearly seen that couple of modes including 9th and 10th modes have significantly low energy compared to the other modes. Fig. 3.17 shows the Fourier spectra of the resulting

modal responses obtained from the vibration measurements by using the MEMD method revealing that the modal responses contain both mono-component as well as mode-mixed signals. For example, it can be observed that the first IMFs in all floors (i.e., first row of Fig. 3.17) are all mono-components. However, other IMFs (i.e., in second and third row of Fig. 3.17) have mode-mixed modal responses.

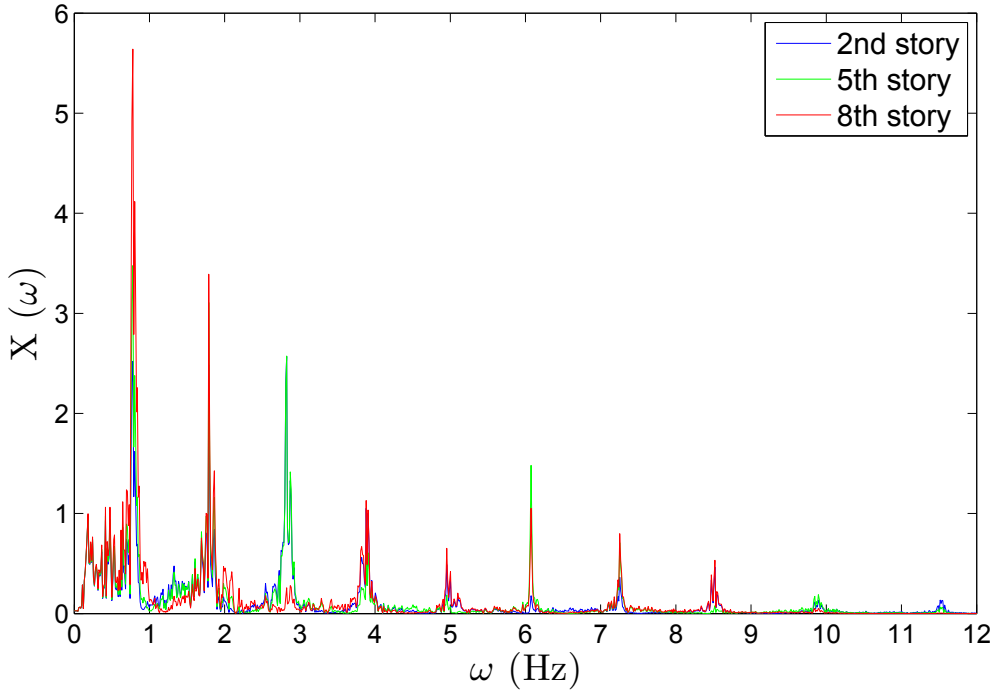

Figure 3.16: Fourier spectra of the floor vibration measurements of the model

In order to extract the mono-component modal responses, the ICA is then applied in the mode-mixed IMFs that are highlighted in red and black boxes. The resulting ICA components (i.e., extracted modal responses) of these IMFs are shown in Fig. 3.18 and Fig. 3.19, respectively. Fig. 3.18 (a), (b) and (c) show the IMFs with mode-mixing resulting from the MEMD that are highlighted in Fig. 3.17 (red box). Fig. 3.18 (e), (f) and (g) show the separated IMFs using the ICA. Also, Fig. 3.19 (a), (b), (d), (e) and (f) show the IMFs with mode-mixing resulting from the MEMD that are highlighted in Fig. 3.17 (blak box). Fig. 3.19 (g), (h), (i), (j), (k) and (l) show the

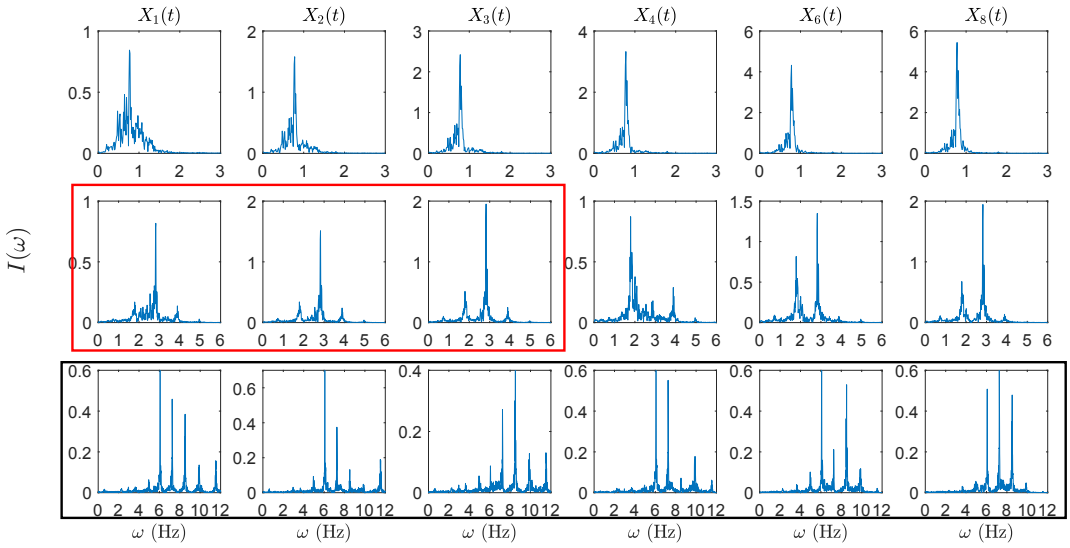

Figure 3.17: IMFs of the first, second, third, fourth, sixth and eighth floor measurements obtained from the MEMD

separated IMFs using the ICA. Consequently, it can be seen that the proposed method has been successfully separated the mode-mixed signals even though the signal has low energy. Table 3.3 shows the identification results revealing the efficiency of the proposed method under a series of low energy and closely-spaced modes.

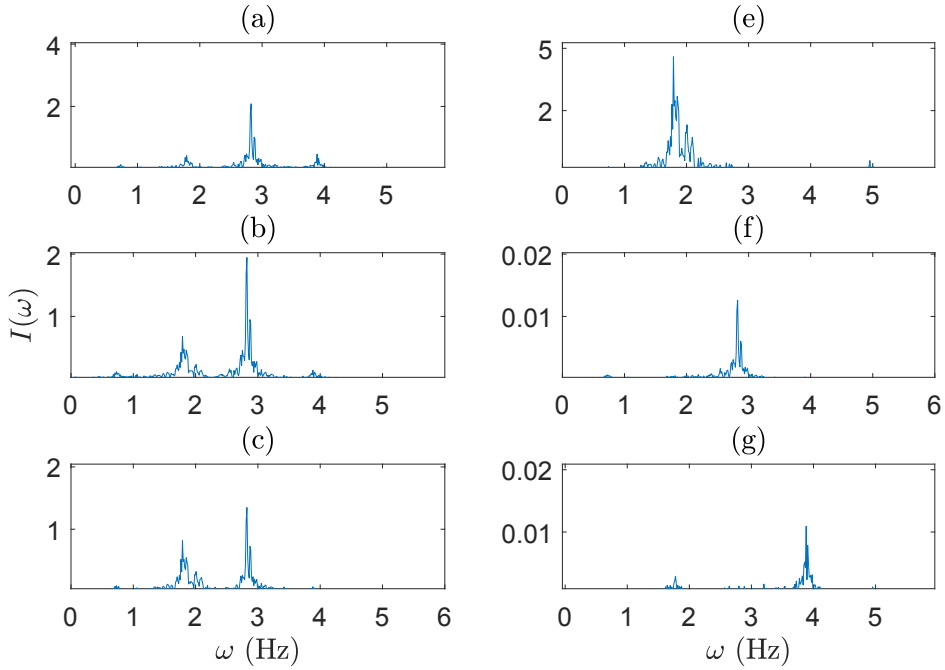

Figure 3.18: (a - b - c) IMFs with mode-mixing and (e - f - g) separated IMFs using the ICA

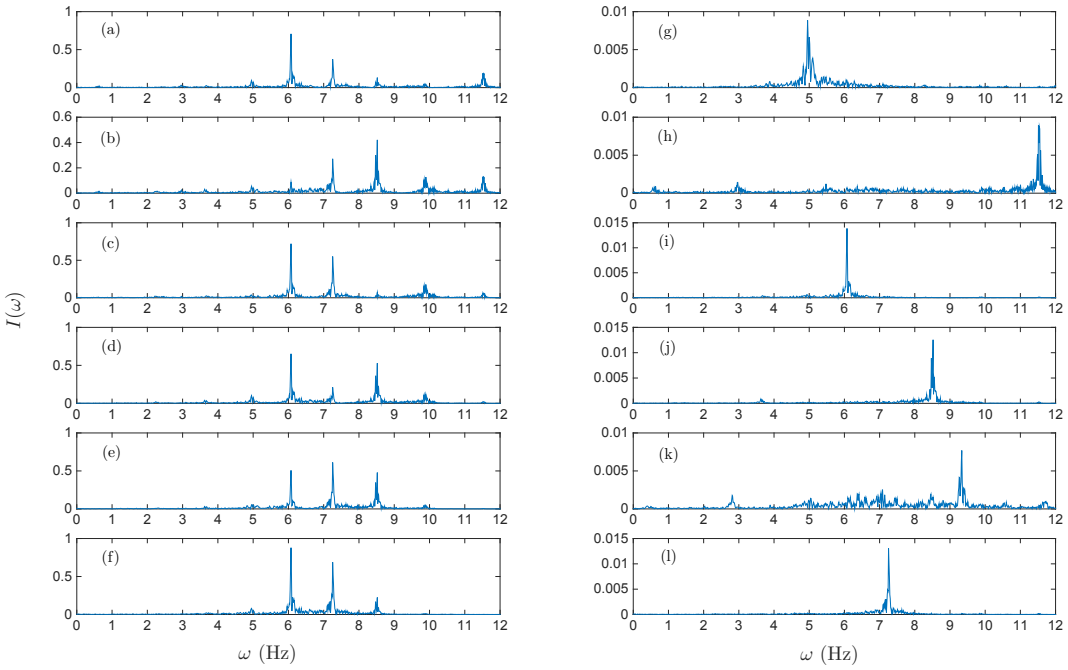

Figure 3.19: (a - b - c - d - e - f) IMFs with mode-mixing and (g - h - i - j - k - l) separated IMFs using the ICA

Table 3.3: Theoretical and identified modal parameters of 10-DOF model

Mode #	1	2	3	4	5	6	7	8	9	10
ω_i (Hz)	0.78	1.79	2.83	3.88	4.96	6.07	7.24	8.49	9.87	11.52
$\hat{\omega}_i$ (Hz)	0.77	1.78	2.82	3.88	4.95	6.07	7.25	8.52	9.89	11.55

Chapter 4

Full-scale Studies

In this chapter, the proposed method is further verified using an experimental model and two real-life structures located in China and Canada. Unlike simulation studies, the identification results obtained from the measured vibration data is now compared with the Finite Element (FE) models.

4.1 Experimental Study

A six-story experimental model is used to validate the proposed method as shown in Fig. 4.1(a). The first three floors of the model have masses of 2.47 kg and the other three floors have masses of 1.12 kg. The model is placed on a shake table which is connected to a shaker manufactured by Crystal Instruments. In order to collect the vibration data, the uniaxial sensors are placed at the middle of each floor of the model, and the sensors are connected to the data acquisition system manufactured by Data Translation attached with a computer. The model is excited using a random shaking for 60 sec via a control system attached to the modal shaker and then the vibration data is collected using the sensors. The S-Frame software of structural analysis is used to develop the FE model as shown in 4.1(b).

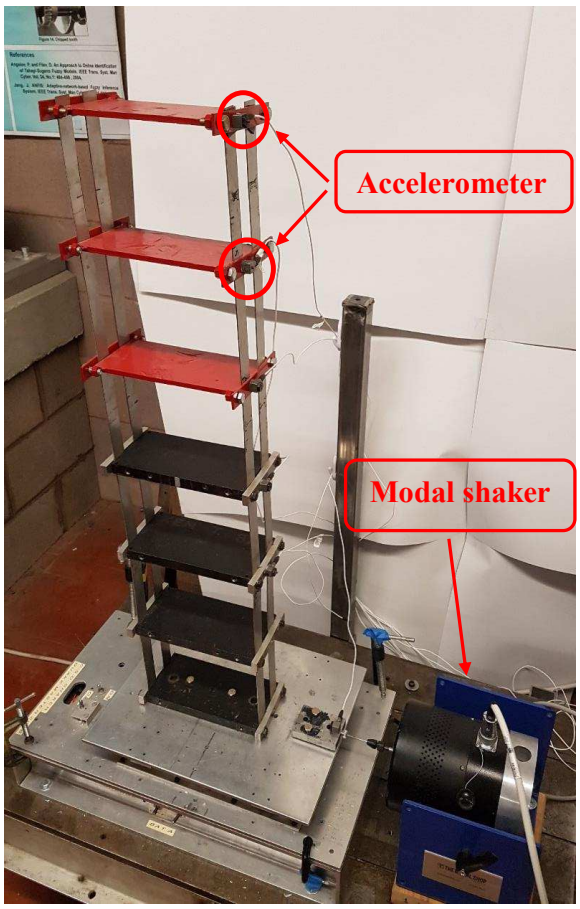

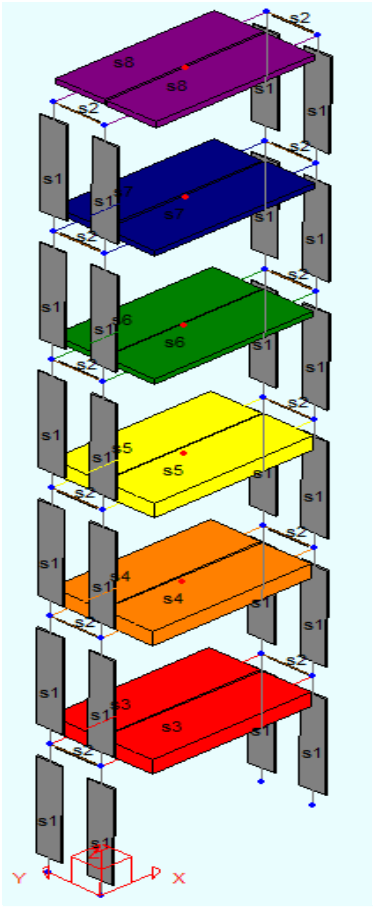

(a) (b)

Figure 4.1: (a) Experimental model and (b) FE model

Fig. 4.2 (a) and (b) show vibration responses of third floor and its corresponding Fourier spectrum, respectively. The vibration data from all floors are then analyzed using the proposed method. Fig. 4.3 shows the Fourier spectra of the modal responses as obtained from the MEMD. It can be observed that IMFs in first and third row of Fig. 4.3 are mono-component. However, IMFs in second and fourth row of Fig. 4.3 have mode-mixed modal responses. The ICA is then applied in the mode-mixed signals (as shown in red box in fourth row of Fig. 4.3) to find the mono-component responses. The resulting ICA components are shown in Fig. 4.4. Fig. 4.4 (a), (b), and (c) show IMFs with mode-mixing of three modal response extracted from MEMD that are shown in Fig. 4.3 (red box). Fig. 4.4 (d), (e) and (f) show the separated IMFs by using the proposed method. Table 4.1 shows the accuracy of the identification results. Fig. 4.5 shows the first six modeshapes of the model and the accuracy of the identified modeshapes are assessed through the modal assurance criteria (MAC) in Table 4.1.

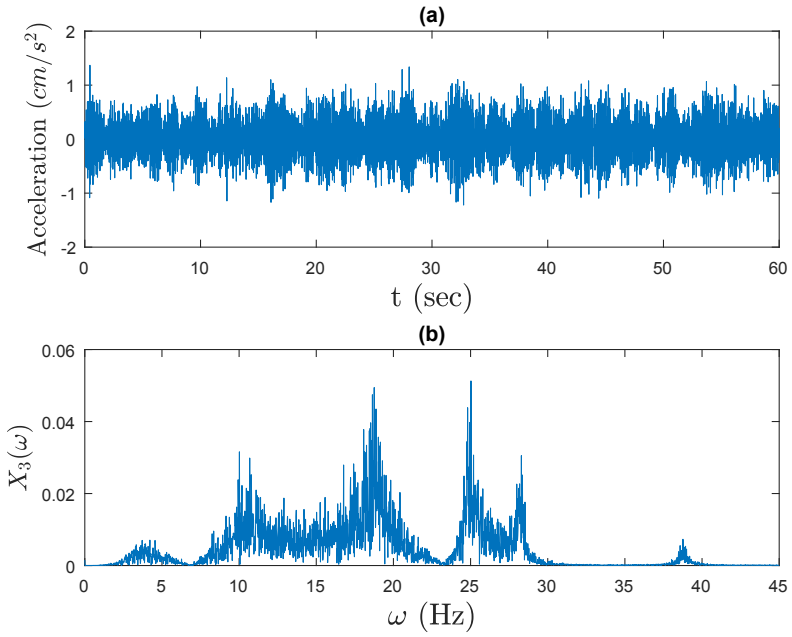

Figure 4.2: (a) Sample data and (b) Fourier spectrum of 3-th floor response

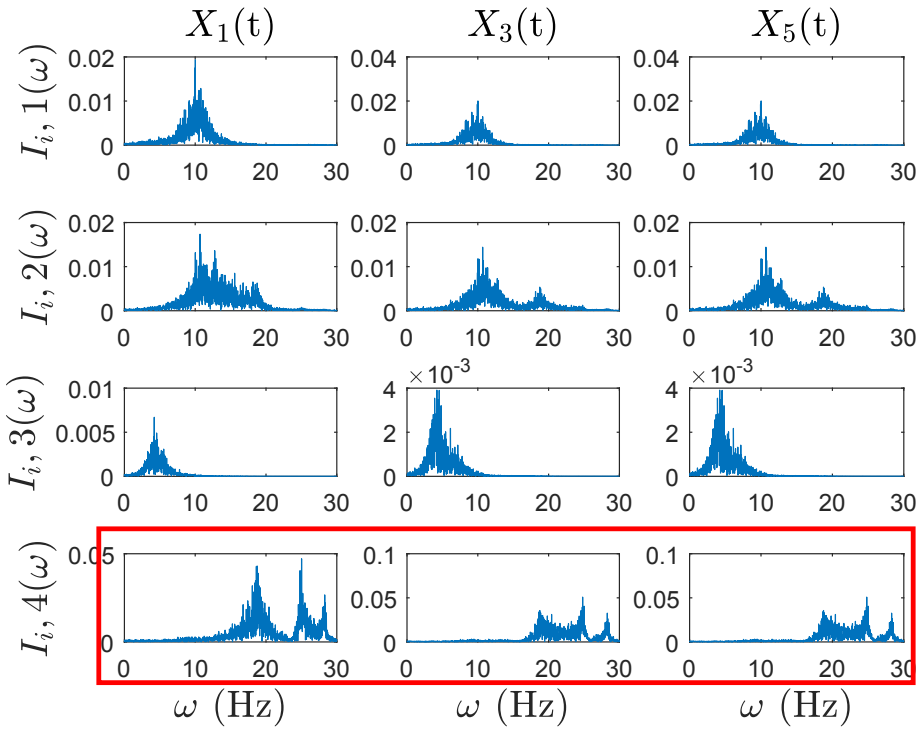

Figure 4.3: IMFs of first, third and fifth sensor as obtained from the MEMD method

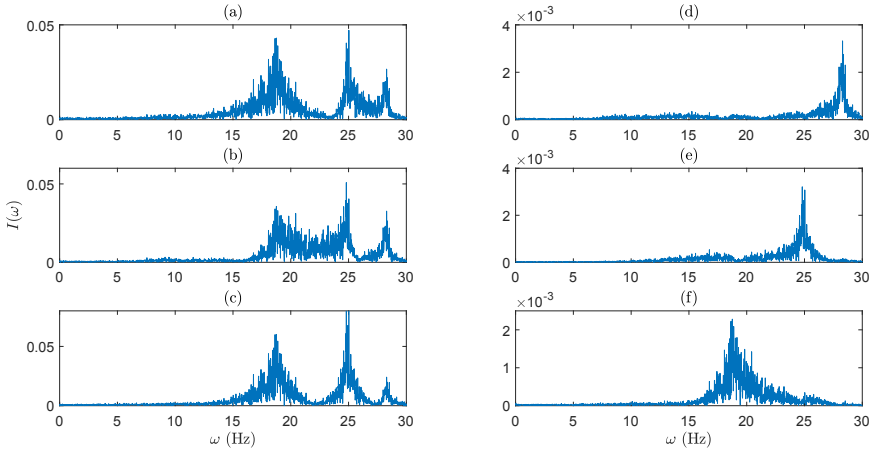

Figure 4.4: (a - b - c) IMFs with mode-mixing and (d - e - f) separated IMFs using the proposed method

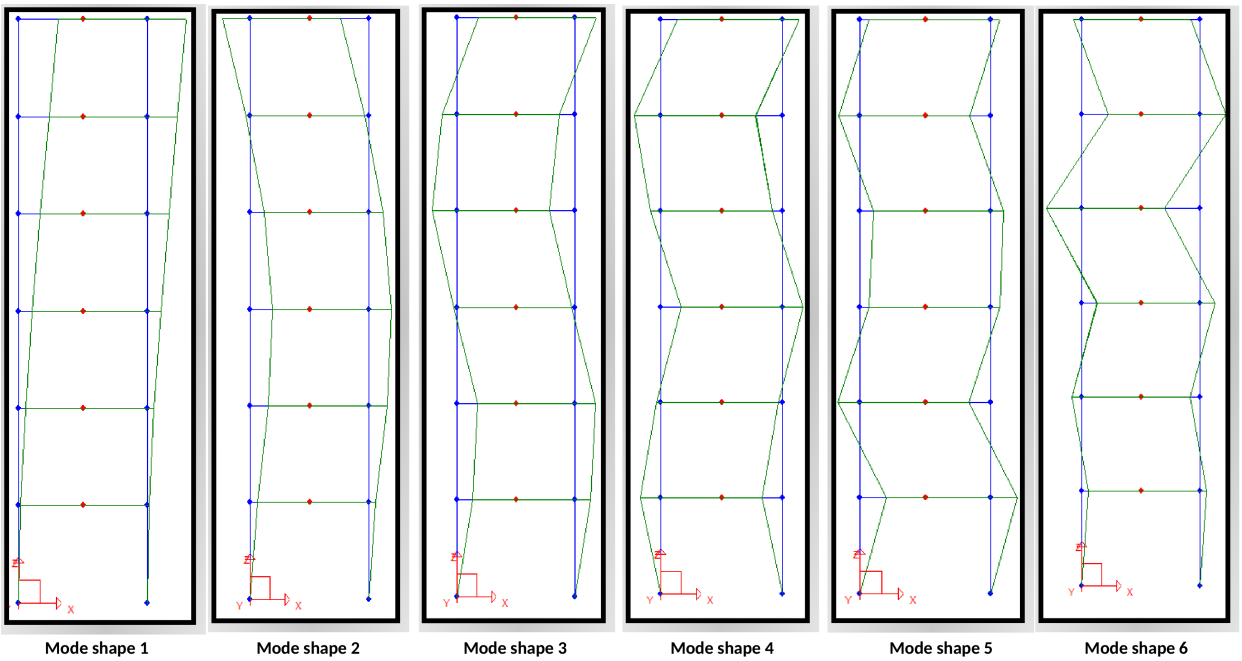

Figure 4.5: Modeshapes of the model

Table 4.1: Accuracy of the identification results in experimental model

Mode #	1	2	3	4	5	6
ω_i	4.6	11.3	18.6	25.6	28.8	39.2
$\hat{\omega}_i$	4.5	10.7	18.7	25.0	28.3	38.7
$\hat{\zeta}_i$ (%)	0.1	0.52	0.73	0.83	0.32	0.053
MAC	1.0	0.99	1.0	0.98	0.98	0.99

4.2 Real-life Structural Validation

The primary focus of this thesis was to perform modal identification of large-scale civil infrastructure such as tall buildings and bridges. Real-life structures undergo a series of dynamic loads that cause significant vibration which can be monitored through multiple sensors installed throughout the premises. In order to validate the proposed method under a wide range of practical challenges with closely-spaced and low energy modal frequencies, two different full-scale structures are selected in this study - (a) a high-rise tower in China and (b) a large-span highway bridge in Canada.

4.2.1 High-rise Tower

The Canton Tower (CT) is located in Guangzhou, China and was constructed in 2010. It stands at a height of 600m with 37 floors [53]. This super-tall structure has experienced several typhoons and earthquake excitation in past few years. The dynamical responses of the tower were successfully collected using a sophisticated monitoring system. However, this study utilizes the vibration data that were collected at the beginning of 2010, shortly after the completion of the CT where no typhoon effect was recognized. This data forms an excellent test bed to validate the proposed algorithm with a large number of DOFs.

Description of the tower

The CT remains the tallest TV tower in the world and it is located in Guangzhou, China. The tower has a slender design with varying cross sectional dimensions throughout as shown in Fig. 4.6 which makes it a unique and aesthetically pleasing modern skyscraper. The main body of the tower is made of reinforced concrete. The bottom of the building is an ellipse shaped cross sectional area at 50 m x 80 m.

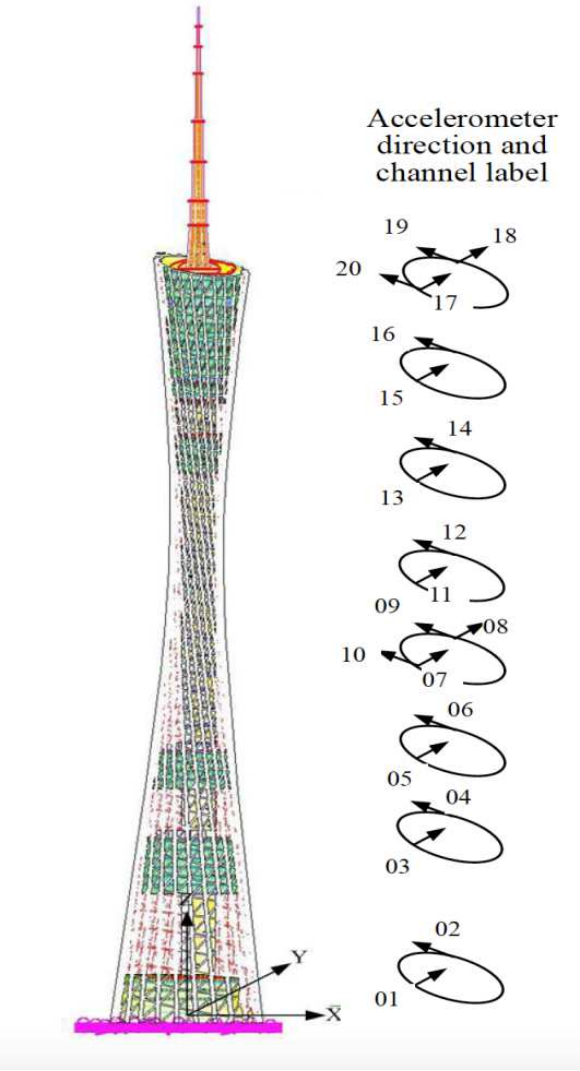

Figure 4.6: Schematic of sensor locations in the Canton Tower (Ni et al. 2009)

At the middle waist of the building, the ellipse shaped cross sectional area decreases to 20.65 m x 27.5 m. Finally, moving to the top portion of the building, the ellipse shaped cross sectional area increases to 41 m x 55 m [60]. In this research, a series of 20 sensors is studied. Additionally, a full-scale FE model was previously developed [53] prior to the construction of the CT, but only the results of the FE model are briefly mentioned to draw meaningful conclusions.

A schematic of 20 accelerometer sensors are shown in Fig. 4.6. Sample vibration data is provided by the Hong Kong Polytechnic University and is released to the

public for research studies. The data was collected for a 24-hour time-frame starting on the day of January 19, 2010 at 18:00 pm and ended on January 20, 2010 18:00 pm. For the temperature data, there was an observed data point per minute of the entire sampling period, which resulted in 1440 varying temperature readings. The sampling frequency of the accelerometer was set to 50 Hz.

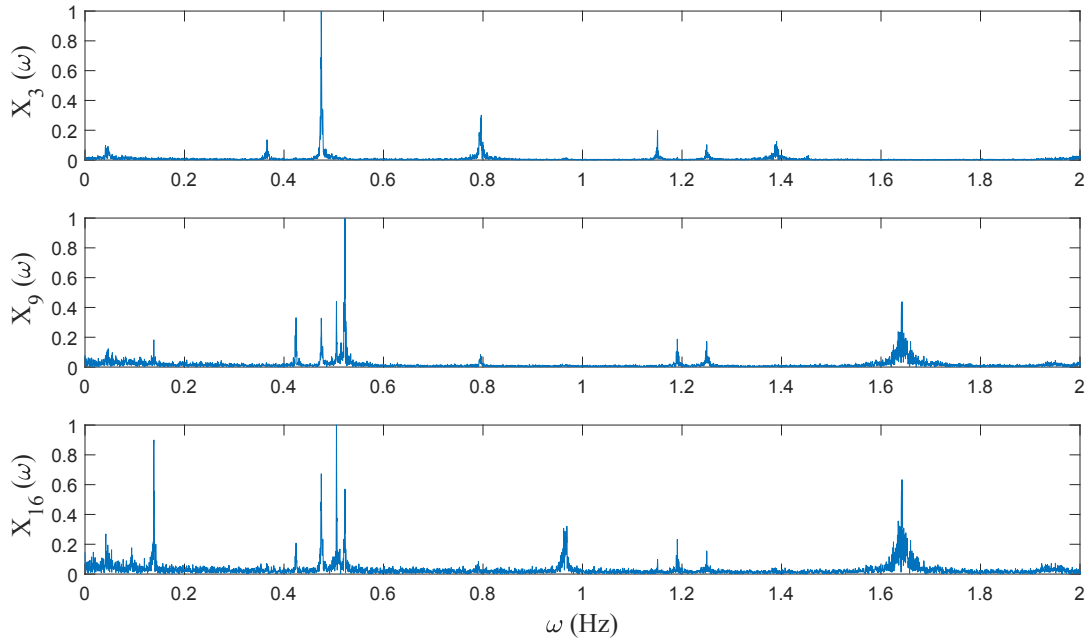

Figure 4.7: Fourier spectra of the vibration measurements at 3rd, 9th and 16th floor

Application of the proposed method

Typical Fourier spectra of sensors along directions 3, 9, and 16 (Fig. 4.6) of January 19, 2010 at 18:00 pm is shown in Fig. 4.7. Fig. 4.8 shows Fourier spectra of the modal responses of the vibration measurements as extracted by the MEMD using this data. In row one and two of Fig. 4.8, it can be observed the IMFs are mono-component. Whereas, the third and fourth rows of Fig. 4.8 contain the mode-mixed modal responses. The ICA is applied in the mode-mixed signal that are highlighted in

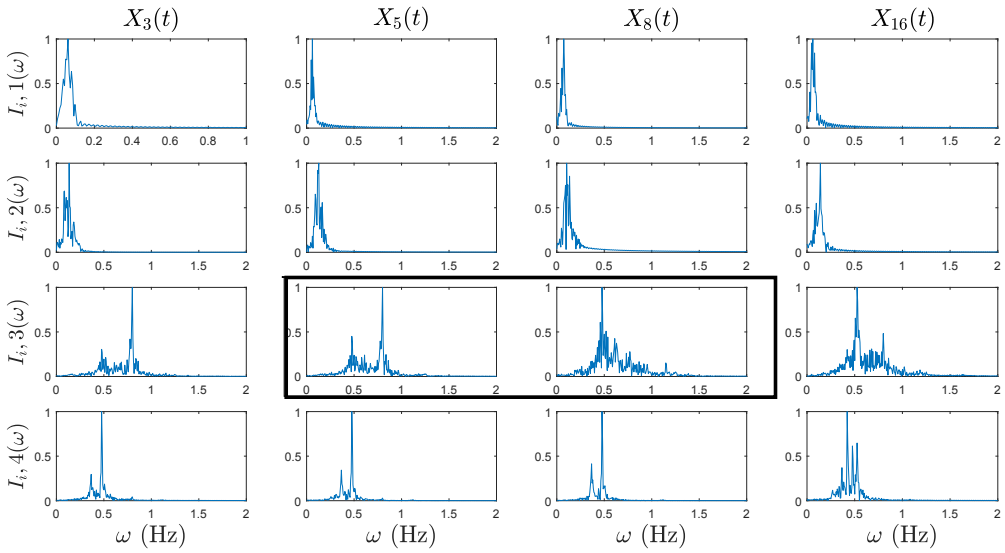

Figure 4.8: IMFs of the third, fifth, eighth and sixteenth sensor as obtained from the MEMD method

black box in third row to get a mono-component. The resulting ICA components are shown in Fig. 4.9 that reveal the separated IMFs and their Fourier spectra. The first column of Fig. 4.9 contains the mode-mixed IMFs that are highlighted in Fig. 4.8 using the black box and the second column contains the separated IMFs as obtained using the ICA.

Similar studies are repeated with the data of entire duration and the daily variation of the natural frequencies is investigated. Table 5.4 shows the variation of natural frequencies for four different hours data and similar exercise is repeated for all 24 hours data. It can be observed that the proposed method has successfully separated the closely-spaced and low energy modes of the CT tower. Fig. 4.10 shows the variation of first two natural frequencies over 24 hours. It may be noted that there is a fluctuation in frequencies (specially in ω_1) due to the change in temperature throughout the day and the difference can be seen in Fig. 4.10. The red lines in Fig. 4.10 present the first two natural frequencies as obtained from the FE model.

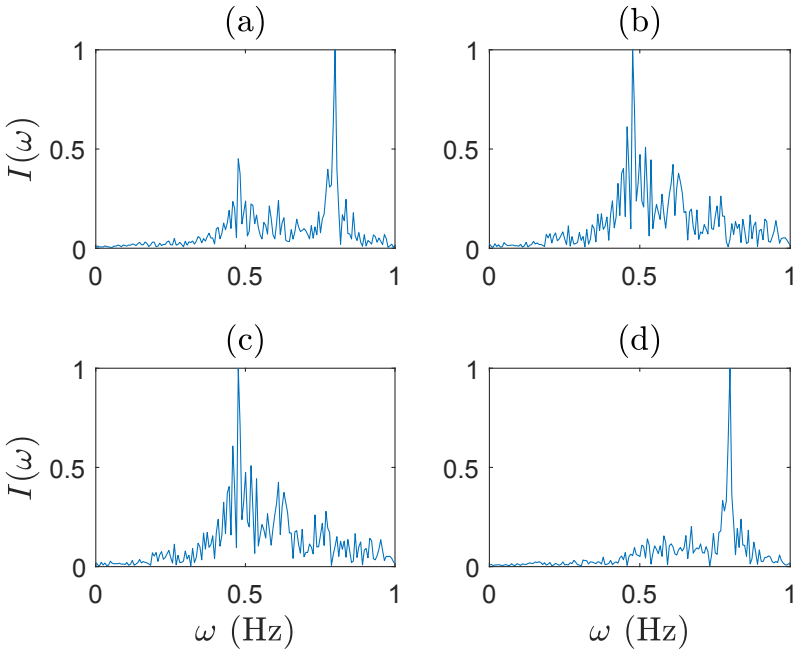

Figure 4.9: (a - c) IMFs with mode-mixing and (b - d) the separated IMFs using the proposed method

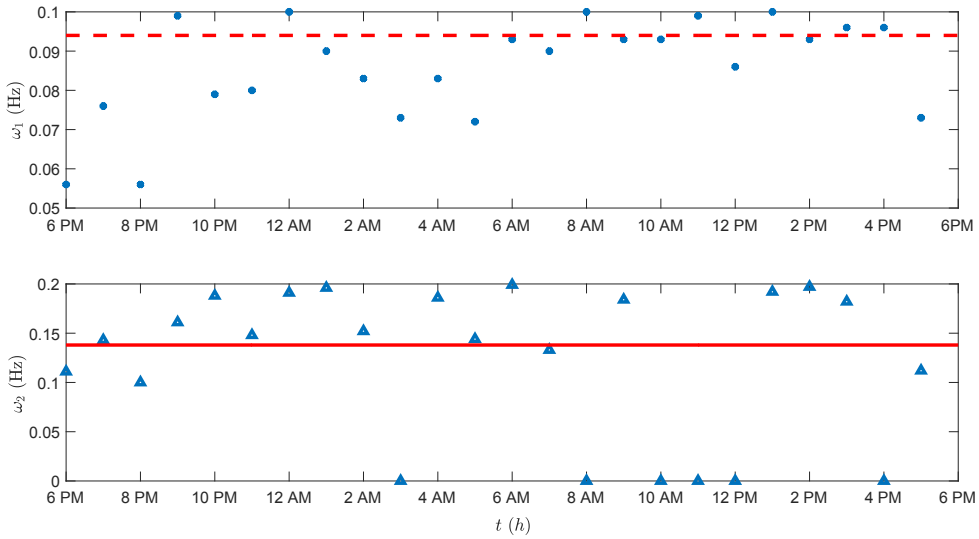

Figure 4.10: Variation of the first two natural frequencies of CT tower over 24 hours

Table 4.2: Daily variation of the identified natural frequencies of the CT tower

ω	Full model	6PM	2AM	9AM	3PM
1	0.094	0.056	0.0083	0.093	0.096
2	0.14	0.11	0.15	0.184	0.182
3	0.29	0.23	0.24	-	0.27
4	0.366	-	-	0.364	-
5	0.474	0.476	0.474	-	0.474
6	0.79	0.8	-	0.8	0.79
7	1.15	1.15	1.15	1.15	-

4.2.2 Long-span bridge

In order to validate the performance of the proposed method, the Main Street bridge located in Thunder Bay, Canada as shown in Fig. 4.11 is utilized. Since its construction, the bridge has seen an increase in heavy traffic (e.g., trucks containing the wind turbine parts) between the Port Authority and the City.

Figure 4.11: Long-span bridge in Thunder Bay

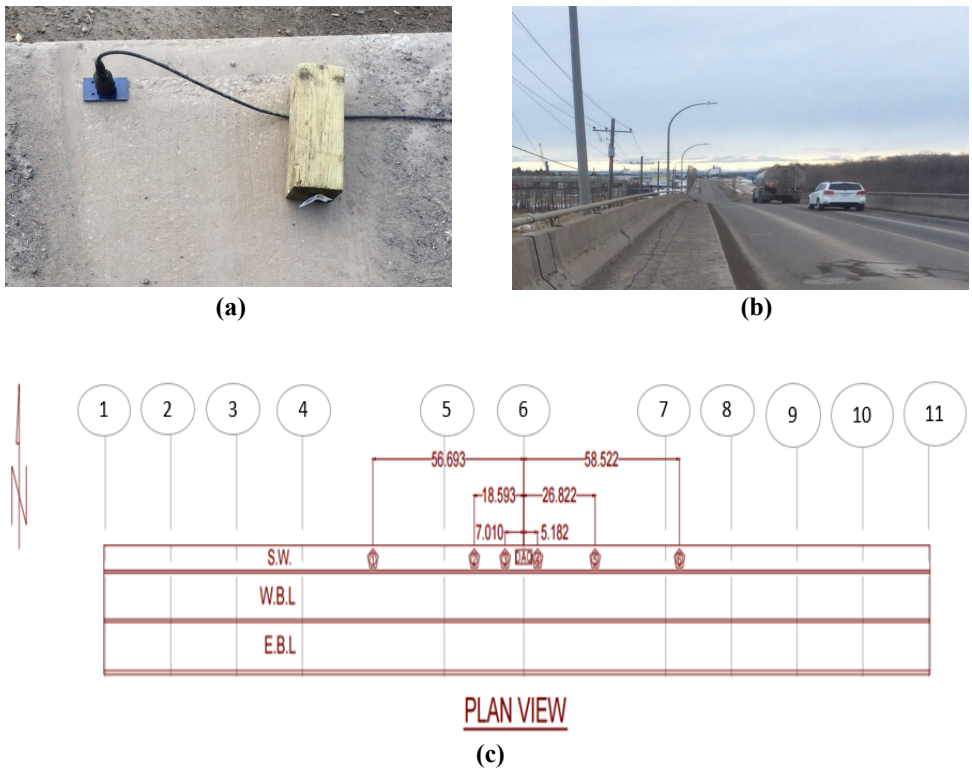

Figure 4.12: (a) Typical sensor placed on the sidewalk, (b) vehicles passing over the bridge during a test and (c) location of sensors on the bridge

Description of the bridge

The Main Street bridge was built in 1960, its length and width are 288 m and 9 m, respectively. The bridge is supported by 11 piers and maximum height of these piers is 8 m and the spacing between piers is 53 m. In order to conduct the serviceability assessment of this bridge, vibration testing was performed on January 20th, 2017 between 9 am - 12 noon. The temperature during the test was approximately $-5°C$. Six sensors were placed along the walkway on the North side of the bridge. Sensors were set up to measure uniaxial vibration in the vertical direction and they were

mounted using the steel plates as shown in Fig. 4.12 (a). The data acquisition (DAQ) system is placed at the centerline of the bridge and the spacing of the sensors were roughly 10, 100 and 200 feet off either side of the DAQ as shown in Fig. 4.12 (c). Several tests were conducted with various numbers of vehicles crossing the bridge at different speeds (50-60 km/h) where the duration of each test was kept between 30 seconds to 2 minutes. Apart from the vibration testing, the FE model of this Bridge is developed using the S-Frame as shown in Fig. 4.13.

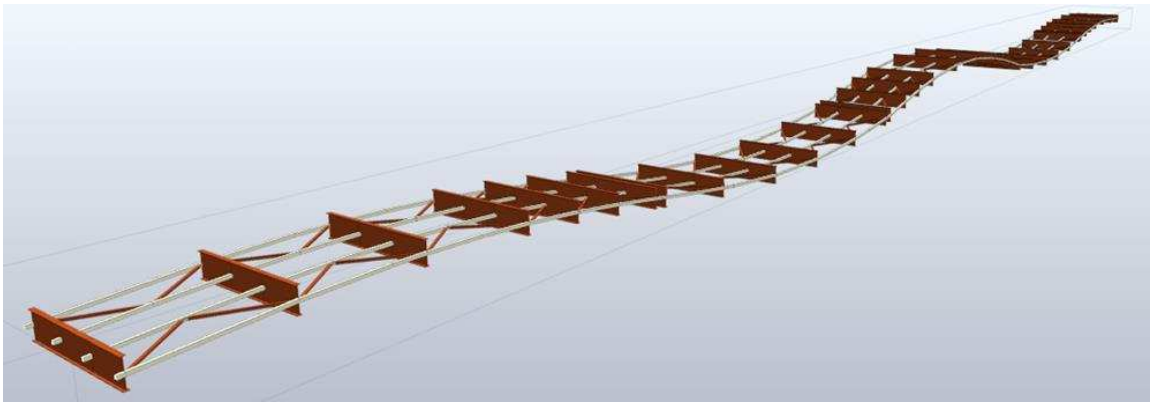

Figure 4.13: FE model of the bridge

The composite section was created using the principles of transformed sections. The calculated section properties were verified by hand calculations. The average depth of beams and web thickness were used as 1.55 m and 10 mm respectively. The calculated section properties from the S-frame were transformed to the material of the lower young's modulus. This meant that when assigning the material properties to the composite section it would be assigned as a concrete section with zero force density. Assigning zero force density was important due to steel and concrete having different densities. Density allocation was accounted for by computing the area of concrete, steel, and asphalt for each girder and applying the unit weight accordingly to obtain an equivalent uniformly distributed load. The values used for the density of concrete, asphalt, and steel are 24, 23.25, and 77 kN/m^3, respectively. When creating

the S-frame model, the materials are considered to be at ambient temperature of approximately $20°C$. Therefore, to get a closer representation of the vibrational data collected from the Main Street bridge, there was a constant temperature load of $-25°C$ applied to the entire span of the bridge to account for any gain in stiffness due to decrease in temperature. By applying this thermal load, the model is assumed to represent a temperature of $-5°C$, which is the temperature during the test. S-View was used to create rendered visuals that show the mode shape vibrating at its natural frequency. The visual provided a more clear representation of the finite element model. This resulted in the rendered image for revision being somewhat of a wired-frame representation.

Table 4.3: Overview of vehicles passing over bridge during each test

Test No	Overview
Test 2: (50km/hr)	2 x large truck (Lake Bound) car + truck (City Bound)
Test 3: (50km/hr)	car + truck (LB) car + dump truck (CB)
Test 4: (60km/hr)	car (LB) car + truck (CB) flatbed transport (LB) transport (LB)
Test 5: (60km/hr)	car (LB) car (CB)
Test 6	truck (LB) 3 x cars (CB)
Test 7	large truck (LB) 3 x cars (LB) 2 x heavy truck (CB) (crossed at same time)
Test 8	4 x cars + transport (CB) 2 x cars (LB)
Test 9	4 x cars (LB) 2 x cars (CB)
Test 10	3 x cars (CB)
Test 11	3 x cars (LB)
Test 12	4 x cars (CB)
Test 13	3 x transports (CB)

Notes:

• Order listed for each test in chronological order in which vehicles passed over bridge.

• Assumed speed for most vehicles was 50-60km/hr. Large Trucks may have been travelling more slowly.

• (CB): City Bound and (LB): Lake Bound.

• Power was provided to the DAQ and laptop computer using a car battery and inverter.

• Radios were used to coordinate the vehicles within our group passing over the bridge.

Application of the proposed method

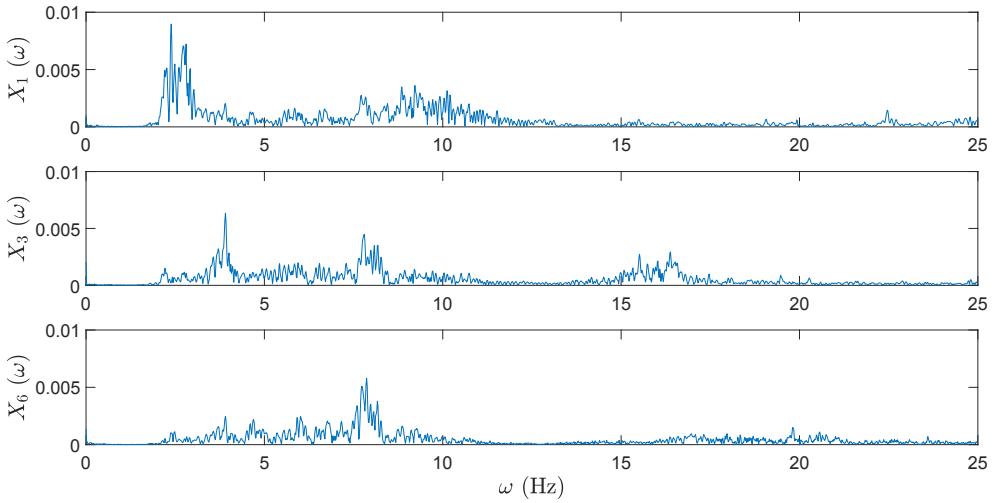

Figure 4.14: Fourier spectra of vibration measurements at various locations

Typical Fourier spectra of three vibration measurements are shown in Fig. 4.14. Fig. 4.15 shows Fourier spectra of the modal responses as obtained by applying the MEMD. The results show modal responses containing both mono-component and mode-mixed signals. It can be observed that the IMFs in row one, three and five of Fig. 4.15 are mono-components. However, the IMFs in second and fourth row of Fig. 4.15 have mode-mixed modal responses. The ICA is applied in the mode-mixed modal responses that are shown in red box in second row to get the modal responses. The resulting ICA components are shown in Fig. 4.16 that reveal the separated IMFs and their Fourier spectra. The first column of Fig. 4.16 contains IMFs with mode-mixed modal responses that are highlighted in Fig. 4.15 (red box) and second column contains the separated IMFs as obtained using the ICA. The resulting modal parameters are compared with their true values in Table 4.4. The

results show that the proposed hybrid MEMD method is able to extract both low energy and closely-spaced frequencies quite accurately.

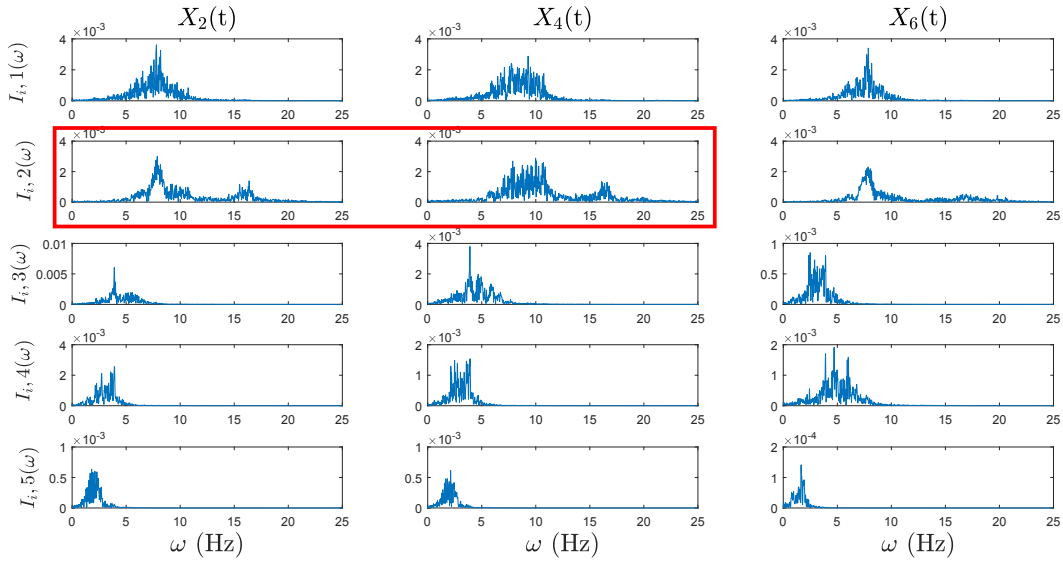

Figure 4.15: The IMFs of the second, fourth and sixth sensor from the MEMD

Table 4.4: Comparison of the identification results with the FE model of long-span bridge

Mode #	1	2	3	4	5	6	7
ω_i (Hz)	2.34	2.4	3.7	5.8	7.6	9.4	16.2
$\hat{\omega_i}$ (Hz)	2.38	2.5	3.9	5.5	7.8	9.9	16
$\hat{\zeta_i}$ (%)	2.3	1.0	0.55	0.4	0.5	0.63	0.1

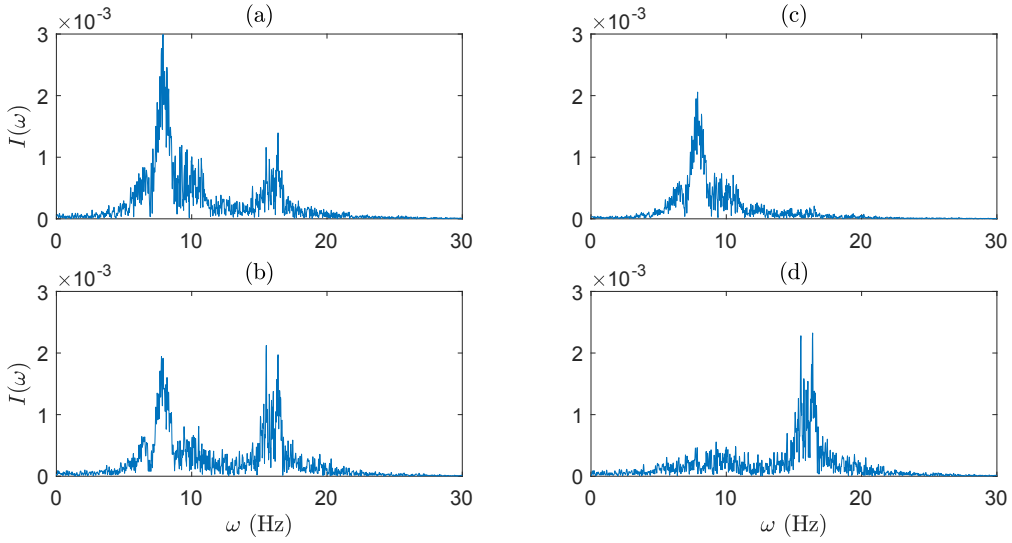

Figure 4.16: The IMFs with mode-mixed modal responses and the separated IMFs using the proposed method

Chapter 5

Conclusions and Future Work

5.1 Key Conclusions

- The MEMD method has been first time explored as a possible candidate for a modal identification method that can deal with multichannel vibration measurements.
- The MEMD method is based on the assumption that the dynamic system has lumped mass degrees-of-freedom. Therefore, while dealing with continuous system, it needs to be discretized as a discrete dynamical system.
- Similar to EMD method, significant mode-mixing is observed in the resulting modal responses as obtained from the MEMD method with the presence of low energy modes, closely-spaced frequencies and measurement noise.
- The mode-mixing problem in the MEMD is resolved by integrating the MEMD with another signal decomposition tool namely ICA. The results show significantly improved performance of the MEMD under a wide range of practical situations.
- The proposed method is validated through a suite of numerical studies employing a broad class of dynamical models and excitation characteristics.
- The practicability of the proposed method is further verified by using an experimental model subjected to base excitation and two real-life full-scale structures

including a high-rise tower and a long-span bridge under ambient vibrations and operational traffic loading, respectively.

5.2 Major Research Contributions

This research has resulted one journal and one conference paper in a leading structural engineering journal and conference, respectively.

1. Sadhu, A. and **Barbosh, M.** (2016). "Structural modal identification using an improved empirical mode decomposition." **CSCE Structures Specialty Conference**, London, Ontario, Canada.

2. **Barbosh, M.**, Sadhu, A. and Vogrig, M. (2017). "Multi-sensor based hybrid empirical mode decomposition method towards system identification of structures." **Journal of Structural Control and Health Monitoring, Wiley**, accepted with minor revisions.

5.3 Future Work

In this thesis, the proposed research is aimed to solve modal identification problems only for linear systems. Following are few potential future work on the MEMD method reserved for our research team:

- The proposed method will be explored for damage detection where the structures are subjected to both discrete and progressive damages.

- The proposed method will be automated to develop a software such that any novice structural engineer can easily deploy this algorithm as a tool in real-time applications.

- The MEMD requires multiple channels of vibration measurements to yield significantly accurate results. In future, the performance of the MEMD will be also explored under limited number of sensor measurements.

- The proposed method will be investigated in structures with torsional modes.

5.4 Acronyms

Following is the list of all relevant acronyms used in this thesis for the convenience of the readers.

SHM	Structural Health Monitoring
SI	System Identification
CE	Complex Exponential
IRF	Impulse Response Function
LSCE	Least-square Complex Exponential
ITD	Ibrahim Time Domain
ERA	Eigen Realization Algorithm
NExT	Natural Excitation Technique
SSI	Stochastic Subspace Identification
FDD	Frequency Domain Decomposition
TMDs	Tuned Mass Dampers
WT	Wavelet Transform
DWT	Discrete Wavelet Transform
CWT	Continuous Wavelet Transform
SWT	Stationary Wavelet Transform
BSS	Blind Source Separation
SOBI	Second-order Blind Identification
ICA	Independent Component Analysis
EMD	Empirical Mode Decomposition
EEMD	Ensemble Empirical Mode Decomposition
MEMD	Multivariate Empirical Mode Decomposition
IMF	Intrinsic Mode Function
DOF	Degrees-of-freedom
FE	Finite Element
DAQ	Data Acquisition

Bibliography

[1] Klikowicz, P., Salamak, M. and Poprawa, G. (2016). "Structural Health Monitoring of Urban Structures." *Procedia Engineering*, 161, 958-962.

[2] Reynders, E. (2012) "System identification methods for (operational) modal analysis: review and comparison." *Archives of Computational Methods in Engineering*, 19.1, 51–124.

[3] Sadhu, A. (2013). "Decentralized ambient modal identification of structures." *PhD Thesis*, Department of Civil and Environmental Engineering, University of Waterloo, Canada.

[4] Hazra, B. (2010). "Hybrid time and time-frequency blind source separation towards ambient system identification of structures." *PhD Thesis*, Department of Civil and Environmental Engineering, University of Waterloo, Canada.

[5] Spitznogle, F. R. and Quazi, A. H. (1970). "Representation and nnalysis of time-limited signals using a complex exponential algorithm." *The Journal of the Acoustical Society of America*, 47:1150–1155.

[6] Ibrahim, S.R. and Mikulcik, E.C. (1973). "A time domain modal vibration test technique." *Shock and Vibration Bulletin*, 43(4):21–37.

[7] Allemang, R.J. and Brown, D.L.(1998). "A unified matrix polynomial approach to modal identification." *Journal of Sound and Vibration*, 211(3):301–322.

[8] Juang, J.N. and Pappa, R.S.(1985). "An eigen system realization algorithm for modal parameter identification and model reduction." *Journal of Guidance, Control and Dynamics*, 8(5):620–627.

[9] Maia, N. M. M. and et. al.(1997). "Theoretical and experimental modal analysis." *Research Studies Press, Taunton, Somerset, UK.*

[10] Asmussen, J. C.(1997). "Modal analysis based on the random decrement technique application to civil enginnering strcutures." *PhD Thesis, Alborg university, Denmark.*

[11] Lin, C. C., Wang, J. F. and Ueng, J.M.(2001). "Vibration control identification of seismically excited m.d.o.f. structure-ptmd systems." *Journal of Sound and Vibration*, 240(1):87–115.

[12] Richardson, M.H. and Formenti, D.L. (1982). "Parameter estimation from frequency response measurements using rational fraction polynomials." *Proceedings of 1st IMAC Conference, Orlando, Florida*, pages 1–15.

[13] James, G.H., Carne, T.G. and Lauffer, J.P.(1995). "The natural excitation technique (NExT) for modal parameter extraction from operating structures." *Modal Analysis*, 10(4):260–277.

[14] Brownjohn, J. M. W.(2003). "Ambient vibration studies for system identification of tall buildings." *Earthquake Engineering and Structural Dynamics*, 32(1):71–95.

[15] Caicedo, J. M., Dyke, S. J. and Johnson, E. A.(2004). "Natural excitation technique and eigensystem realization algorithm for phase i of the iasc-asce benchmark problem:Simulated data" *J. Engrg. Mech*, 130(1):49–60.

[16] VanOverschee, P. and De Moor, B.(1993). "N4sid: numerical algorithms for state space subspace system identification" *Proceedings of the IFAC World Congress*, pages 361–364.

[17] VanOverschee, P. and De Moor, B.(1996). "Subspace identification for linear systems: Theory, Implementation, Applications." *Dordrecht, Netherlands*.

[18] Skolnik, D., Lei, Y., Yu, E. and Wallace, J.(2006). "Identification, model updating, and response prediction of an instruemented 15-story steel-frame building." *Earthquake Spectra*, 22(3):781–802.

[19] El-Kafafy, M., Guillaume, P., Peeters, B., Marra, F., and Coppotelli, G. (2012). "Advanced frequency-domain modal analysis for dealing with measurement noise and parameter uncertainty." *Conference Proceedings of the Society for Experimental Mechanics Series*, pages 179–199.

[20] Zhang, L., Kanda, H., Brown, L. D. and Allemang, J. R.(1985). "Frequency domain poly-reference method for modal analysis." *Journal of Applied Mechanics*, ASME, 106(85).

[21] Brincker, R., Zhang, L. and Anderson, P.(2001). "Modal identification of output-only systems using frequency domain decomposition." *Smart Materials and Structures*, 10(3):441–445.

[22] Brincker, R., Zhang, L. and Anderson, P.(2000). "Modal identification from ambient responses using frequency domain decomposition." *In Proceedings of the Inter- national Modal Analysis Conference(IMAC)*, San Antonio, Texas, USA.

[23] Brincker, R., Ventura, C. E. and Anderson, P.(2001). "Damping estimation by frequency domain decomposition." *In Proceedings of SPIE, the International Society for Optical Engineering*, volume 4359, pages 698–703.

[24] Carlos, A. P., Juan, P. A., Hojjat, A., Martin, V., Rene, d. R., Aurelio, D. and Roque, A. O.(2016). "Time-frequency techniques for modal parameters identification of civil structures from acquired dynamic signals." *Journal of Vibroengineering* , 18(5), 3164-3185.

[25] Hou, Z., Noori, M. and Amand, R. S. (2000). "Wavelet-based approach for structural damage detection." *J. Engrg. Mech*, 126(7).

[26] Kijewski, T. and Kareem, A. (2003). "Wavelet transforms for system identification in civil engineering." *Computer-Aided Civil and Infrastructure Engineering*,18(5), 339–355.

[27] Hera, A. and Hou, Z. (2004). "Application of wavelet approach for ASCE structural health monitoring benchmark studies." *J. Engrg. Mech*, 130(1), 96–104.

[28] Ghanem, R. and Romeo, F. (2000). "A wavelet based approach for the identification of linear time-varying dynamical systems." *Journal of Sound and Vibration*, 234(4), 555–576.

[29] Taha, M. M. (2006). "Wavelet transform for structural health monitoring: a compendium of uses and features." *Structural Health Monitoring*, 5(3), 267-295.

[30] Lardies, J. and Gouttebroze, S. (2002). "Identification of modal parameters using the wavelet transform." *International Journal of Mechanical Science*, 44:2263–2283.

[31] Yang, Y. and Nagarajaiah, S. (2012). "Time-frequency blind source separation using independent component analysis for output-only modal identification of highly-damped structures." *Journal of Structural Engineering*, 139, 1780–1793.

[32] Antoni, J. and Chauhan, S. (2013). "A study and extension of second-order blind source separation to operational modal analysis." *Journal of Sound and Vibration*, 332(4), 1079–1106.

[33] Sadhu, A., Narasimhan, S. and Antoni, J. (2017). "A review of output-only structural mode identification literature employing blind source separation methods." *Mechanical Systems and Signal Processing*, 94, 415–431.

[34] Hazra, B., Sadhu, A., Roffel, A. J. and Narasimhan, S. (2012). "Hybrid time-frequency blind separation towards ambient system identification of structures." *Computer Aided Civil and Infrastructure Engineering*, 27(5):314–332.

[35] Pines, D. and Salvino, L. (2006). "Structural health monitoring using empirical mode decomposition and the Hilbert phase." *Journal of Sound and Vibration*, 294, 97124.

[36] Geng, C., Wang, F., Z. J. and Jin, Z. (2014). "Modal parameter identification of power transformer winding based on improved empirical mode decomposition method." *Electric Power Systems Research*, 108, 331–339.

[37] Sadhu, A. (2015). "An integrated multivariate empirical mode decomposition method towards modal identification of structures." *Journal of Vibration and Control*

[38] Huang, N. E., Shen, Z., Long, R., Wu, M. C., Shih, H. H., Zheng, Q., Yen, N-C., Tung, C. C. and Liu, H. H. (1998). "The empirical mode decomposition and the Hilbert spectrum for nonlinear and non-stationary time series analysis." *Proceedings of the Royal Society A: Mathematical, Physical and Engineering Sciences*, 454.1971, 903–995.

[40] Wickerhauser, M.V. (1994). "Adapted wavelet analysis from theory to software." *A. K. Peters, Ltd., Wellesley, Massachusetts.*

[41] Fowler, J.E. (2005). "The redundant discrete wavelet transform and additive noise." *Signal Processing Letters*, 12(9):629–632.

[42] Nason, G.P. and Silverman, B.W. (1995). "The stationary wavelet transform and some statistical applications." *Lecture Notes in Statistics.*

[43] Mallat, S. G. (1998). "A Wavelet tour of signal processing." *Academic Press, San Diego.*

[43] Cichocki, A. and Amari, S. (2003). "Adaptive blind signal and image processing." *John Wiley and Sons, Ltd., Wiley (West Sussex), UK*

[44] Belouchrani, A., Abed-Meraim, K., Cardoso, J.F. and Moulines, E. (1997). "A blind source separation technique using second-order statistics." *IEEE Transactions on signal processing*, 45(2):434–444.

[45] Sadhu, A., Narasimhan, S. and Antoni, J. (2017). "A literature review of output-only structural modal identification employing blind source separation methods." *Mechanical Systems and Signal Pocessing*, Elsevier, 94, 415-431.

[46] Rehman, N. and Mandic, D. P. (2010). "Multivariate empirical mode decomposition." *Proceedings of The Royal Soceity A*, 466, 1291–1302.

[47] Lv, Y., Yuan, R. and Song, G. (2016). "Multivariate empirical mode decomposition and its application to fault diagnosis of rolling bearing." *Mechanical Systems and Signal Processing*, 81, 219-234.

[48] Rehman, N., Ehsan, S., Abdullah, S. M., Akhtar, M. J., Danilo, P. M. and Klaus, D. M. (2015). "Multi-scale pixel-based image fusion using multivariate empirical mode decomposition." *Sensors*, 15, 10923–10947.

[49] Comon, P. (1994). "Independent component analysis: a new concept?" *Signal Processings*, 36:287–314.

[50] Hyvarinen, A. and Oja, E. (2000). "Independent component analysis: algorithms and applications." *Neural Networks Research Centre Helsinki University of Technology*, 13(45), 411–430.

[51] Hyvarinen, J. A. Karhunen, and Oja, E. (2001) "Independent component analysis." *John Wiley, New York.*

[52] Le, T. and Paultre, P. (2012). "Modal identification based on continuous wavelet transform and ambient excitation tests." *Journal of Sound and Vibration*, 331, 2023-2037.

[53] Ni, Y. Q., Xia, Y., Liao, W. Y., and Ko, J. M. (2009). "Technology innovation in developing the structural health monitoring system for Guangzhou new Tv tower." *Structural control and Health Monitoring*, 16, 73–98.

[54] Moore, K. J., Kurt, M., Eriten, M., McFarland, D. M., Bergman, L. A. and Vakakis, A. F. (2017). "Wavelet-bounded empirical mode decomposition for measured time series analysis." *Mechanical Systems and Signal Processing*, 99, 14–29.

[55] Hyvarinen, A. (2012). "Independent component analysis: recent advances." *Signal Processing and Inference for the Physical Sciences*, 371: 20110534.

[56] Yang, J. N., Lei, Y., Lin, S. and Huang, N. (2004). "Hilbert-Huang Based Approach for Structural Damage Detection." *Journal of Engineering Mechanics*, 130(1): 85–95.

[57] Zheng, J., Cheng, J. and Yang, Y. (2014). "Partly ensemble empirical mode decomposition: An improved noise-assisted method for eliminating mode mixing." *Signal Processing*, 96, 362–374.

[58] Sungkono, Ayi, S. B., Dwa, D. W., Fernando, A. M. and Bagus, J. S. (2014). "Fast, simultaneous and robust VLF-EM data denoising and reconstruction via multivariate empirical mode composition." *Computers and Geosciences*, 67, 125–138.

[59] Syed, K. B. and Mohammed, I. H. B. (2016). "Classification of motor imagery movements using multivariate empirical mode decomposition and short time Fourier transform based hybrid method." *Engineering Science and Technology, an International Journal*, 19, 457–464.

[60] Liao, W. (2012). "Comfort assessment of tower-like slender structures under typhoons and earthquakes." *PhD Thesis , Department of Civil and Structural Engineering. The Hong Kong Polytechnic University. Hong Kong: Pao Yue-Kong Library.*